The July 2019 European heatwave in a warmer climate: Storyline scenarios with a coupled model using spectral nudging

Antonio Sánchez Benítez[1], Helge Goessling[1], Felix Pithan[2], Tido Semmler[1], and Thomas Jung[1]

[1]Alfred Wegener Institute Helmholtz-Center for Polar and Marine Research, Bremerhaven, Germany
[2]Alfred Wegener Institute Helmholtz-Center for Polar and Marine Research, Bremerhaven, Germany.

November 23, 2022

Abstract

Extreme weather events are triggered by atmospheric circulation patterns and shaped by slower components, including soil moisture and sea-surface temperature, and by the background climate. This separation of factors is exploited by the storyline approach where an atmosphere model is nudged toward the observed dynamics using different climate boundary conditions to explore their influence. The storyline approach disregards rather uncertain climatic changes in the frequency and intensity of dynamical conditions, but focuses on the thermodynamic influence of climate on extreme events. Here we demonstrate an advanced storyline approach that employs a coupled climate model (AWI-CM-1-1-MR) where the large-scale free-troposphere dynamics are nudged toward ERA5 data. Five-member ensembles are run for present-day (2017–2019), pre-industrial, +2K, and +4K climates branching off from CMIP6 historical and scenario simulations of the same model. In contrast to previous studies, which employed atmosphere-only models, feedbacks between extreme events and the ocean and sea-ice state, and the dependence of such feedbacks on the climate, are consistently simulated. Our setup is capable of reproducing observed anomalies of relevant unconstrained parameters, including near-surface temperature, cloud cover, soil moisture, sea-surface temperature, and sea-ice concentration. Focusing on the July 2019 European heatwave, we find that the strongest warming amplification expands from southern to central Europe over the course of the 21st century. The warming reaches up to 10 K in the 4K warmer climate, suggesting that an analogous event would entail peak temperatures around 50 °C in central Europe.

3   **The July 2019 European heatwave in a warmer climate: Storyline**

4   **scenarios with a coupled model using spectral nudging**

5   Antonio Sánchez-Benítez,[a] Helge Goessling,[a] Felix Pithan,[a] Tido Semmler, [a] Thomas Jung,[a,b]

6   [a] Alfred Wegener Institute Helmholtz-Center for Polar and Marine Research, Bremerhaven, Germany.

7   [b] *University of Bremen, Institute of Environmental Physics, Bremen, Germany*

8

9   *Corresponding author*: Antonio Sánchez-Benítez, antonio.sanchez.benitez@awi.de

1

10   ABSTRACT

11   Extreme weather events are triggered by atmospheric circulation patterns and shaped

12   by slower components, including soil moisture and sea-surface temperature, and by the

13   background climate. This separation of factors is exploited by the storyline approach where an

14   atmosphere model is nudged toward the observed dynamics using different climate boundary

15   conditions to explore their influence. The storyline approach disregards rather uncertain

16   climatic changes in the frequency and intensity of dynamical conditions, but focuses on the

17   thermodynamic influence of climate on extreme events. Here we demonstrate an advanced

18   storyline approach that employs a coupled climate model (AWI-CM-1-1-MR) where the large-

19   scale free-troposphere dynamics are nudged toward ERA5 data. Five-member ensembles are

20   run for present-day (2017–2019), pre-industrial, +2K, and +4K climates branching off from

21   CMIP6 historical and scenario simulations of the same model. In contrast to previous studies,

22   which employed atmosphere-only models, feedbacks between extreme events and the ocean

23   and sea-ice state, and the dependence of such feedbacks on the climate, are consistently

24   simulated. Our setup is capable of reproducing observed anomalies of relevant unconstrained

25   parameters, including near-surface temperature, cloud cover, soil moisture, sea-surface

26   temperature, and sea-ice concentration. Focusing on the July 2019 European heatwave, we find

27   that the strongest warming amplification expands from southern to central Europe over the

28   course of the 21st century. The warming reaches up to 10 K in the 4K warmer climate,

29   suggesting that an analogous event would entail peak temperatures around 50 ℃ in central

30   Europe.

31

32

33

34   SIGNIFICANCE STATEMENT

35   This work explores a new storyline method to determine the impact of climate change

36   on specific recent extreme events. The observed evolution of the large-scale atmospheric

37   circulation is imposed in a coupled climate model. Variations in climate parameters, including

38   ocean temperatures and sea ice, are well reproduced. By varying the background climate,

39   including CO_2 concentrations, it is demonstrated how the July 2019 European heatwave could

40   have evolved in pre-industrial times and in warmer climates. For example, up to 10 °C warmer

41   peak temperatures could occur in central Europe in a 4 °C warmer climate. The method should

42   be explored for other types of extreme events and has the potential to make climate change

43   more tangible and to inform adaptation measures.

44   **1. Introduction**

45   Europe has recently experienced a number of exceptional heatwaves (e.g., Russo et al.

46   2015; Vautard et al. 2020). These extreme events matter for society as they are associated,

47   among others, with extensive crop failures (Lesk et al. 2016; Beillouin et al. 2020), devastating

48   wildfires (Sutanto et al. 2020), poor air quality (e.g., Konovalov et al. 2011; Garrido-Perez et

49   al. 2019), and increased mortality, especially in the older people (Barriopedro et al. 2011;

50   CRED 2020). The most extensively documented heatwaves – both in terms of studying the

51   underlying dynamics and associated impacts – are the August 2003 heatwave over western and

52   central Europe (e.g., Trigo et al. 2005; Russo et al. 2015; Bador et al. 2017) and the July–

53   August 2010 event in western Russia (e.g., Barriopedro et al. 2011; Dole et al. 2011). These

54   heatwaves redrew the temperature record map of Europe. More recently, the 2019 summer was

55   exceptional in western and central Europe (Mitchell et al. 2019; Madruga De Brito et al. 2020;

56   Sousa et al. 2020; Vautard et al. 2020) with two large-scale heatwaves occurring in late June

57   and July 2019. These two extreme events were found to be the world's deadliest disaster of

3

58   2019 (CRED 2020). The former set a new record for the European-average June temperature.

59   The most extreme daily maximum 2m air temperature (t2m) was recorded on 28 June near the

60   city of Nimes (Verargues, 46 ℃), where a new all-time national record for France was

61   established. The latter resulted in record-breaking temperatures in central and northern Europe.

62   For example, the historical record of Paris was broken by more than 2 ℃ (42.6 ℃); Belgium

63   and the Netherlands for the first time surpassed the 40 ℃ mark; and new national records were

64   set in Germany, Luxembourg and the UK.

65   There is consensus that large-scale dynamics, characterized by subtropical ridges and

66   blocking anticyclones associated with meandering of the jet stream, are the main driving factor

67   for European heatwaves (e.g., Trigo et al. 2005; Jézéquel et al. 2018; Sánchez-Benítez et al.

68   2018; Sousa et al. 2020; Suarez-Gutierrez et al. 2020) as warm air advection from lower

69   latitudes, solar radiative heating and subsidence are enhanced. The 2003 and 2019 heatwaves

70   were associated with a subtropical ridge in western Europe together with a low-pressure system

71   in the eastern Atlantic. This configuration advected hot and dry Saharian and Iberian air masses

72   towards higher latitudes. Soil-atmosphere feedbacks impacted the strength of the heatwaves

73   (e.g., van der Wiel et al. 2020) as they generate changes in the surface heat fluxes (Wehrli et

74   al. 2018; Miralles et al. 2019; Sousa et al. 2020). In fact, the heatwaves in August 2003 and

75   July 2019 were preceded by anomalously warm and dry conditions, generating a soil moisture

76   deficit. For this type of event, other mechanisms, for example involving local SST, are believed

77   to be of less relevance, although some controversy remains (Della-Marta et al. 2007; Duchez

78   et al. 2016; Wehrli et al. 2019).

79   The Mediterranean region is often referred to as a hotspot of climate change due to a

80   substantial amplification of global warming, especially in summer (Fischer and Schär 2010;

81   Barcikowska et al. 2020). The amplification can partly be explained by a substantial decrease

4

82   in soil moisture availability. In future warmer climates, this lack of soil moisture – and hence

83   the amplification – is expected to propagate northward, impacting central Europe (Vogel et al.

84   2017; Suarez-Gutierrez et al. 2020; Wehrli et al. 2020). Overall, it is now well established that

85   climate change has made heatwaves more frequent, intense and prolonged (Chapman et al.

86   2019; Perkins-Kirkpatrick and Lewis 2020; Sánchez-Benítez et al. 2020); and this trend is

87   expected to continue in the future (Schoetter et al. 2015; Junk et al. 2019; Suarez-Gutierrez et

88   al. 2020).

89   Climate models and observations have been used to quantify how the odds of extreme

90   temperatures that occurred during specific heatwaves have changed from the past and how

91   much they will change in the future (e.g., Vogel et al. 2019; Zhou et al. 2019; Vautard et al.

92   2020). For example, an event like the July 2019 heatwave in France (Germany) is now

93   considered to be at least ten (three) times more likely to occur than in 1900 (Vautard et al.

94   2020); and such an extreme event will be ~150 times more probable by the end of the century

95   for the SSP585 scenario (i.e., 1.8 vs. 273 years return period by the end of the 21st century

96   compared to 1950–2014; Ma et al. 2020). Despite some obvious successes of this *probabilistic*

97   *approach*, as argued by Shepherd (2016), it has some limitations: Firstly, projected changes of

98   the polar jet stream in a warmer climate are still highly uncertain (e.g., Shepherd 2014; Hoskins

99   and Woollings 2015; Woollings et al. 2018). Hence, large ensembles are needed to provide

100   meaningful statements. Furthermore, it is rather difficult to find good future analogues of

101   heatwaves, not least given that in terms of impacts (e.g., on hydrology) the temporal evolution

102   of the system prior to the heatwave is critical as well. Secondly, the probabilistic approach does

103   not make the anticipated changes in a warming world readily accessible to the general public

104   and some decision-makers; this is in stark contrast to so-called storyline scenarios – explored

105   in this study – where the impact of climate change is illustrated by considering recent extreme

106   events that people have experienced and can connect to (Shepherd et al. 2018).

107   The storyline approach provides a way to disentangle dynamic from thermodynamic

108   changes and has been explored in several recent studies (Schubert-Frisius et al. 2017; Shepherd

109   et al. 2018; Wehrli et al. 2020; Van Garderen et al. 2021). In contrast to possible dynamic

110   changes (e.g., meandering of the jet stream), thermodynamic changes associated with

111   heatwaves in a warmer world are better understood and associated with relatively small

112   uncertainty (Cattiaux et al. 2015; IPCC, 2018; Fan et al. 2020). Increasing CO_2 concentrations,

113   for example, are known to warm near-surface temperatures locally; and warmer SSTs lead to

114   enhanced warm-air advection to downstream land regions (e.g., Dommenget 2009). In the

115   deterministic storyline approach, heatwaves are simulated in alternative past and future

116   climates, using an atmospheric general circulation model in which the dynamics in the free

117   troposphere are nudged towards observations using reanalysis data. These simulations start

118   some years before the event to appropriately capture the evolution preceding the events (e.g.,

119   spinning up soil hydrology).

120   So far, two different approaches were used for nudging. In Wehrli et al. (2020) the zonal

121   and meridional winds were nudged; meanwhile, in Van Garderen et al. (2021), divergence and

122   vorticity truncated at T20 (spectral nudging) were employed to impose the large-scale

123   dynamical evolution. As both studies used an atmospheric circulation model, the sea-surface

124   temperatures (SST) and sea-ice concentration (SIC) had to be prescribed. For the present-day

125   simulations, the observed SST and SIC, including the variability possibly impacting the

126   considered extreme events, were prescribed. For the past and future climate conditions, a

127   climate change signal was added to the SSTs. This is a reasonable approach as it preserves the

128   variability. However, it implies that one needs to rely on the climate change response of a

6

129 separate, coupled configuration of the same (or similar) atmosphere model, as in Van Garderen

130 et al. (2021), or on the response of one or more completely different climate models, as in

131 Wehrli et al. (2020). The atmosphere-only storyline approach also assumes that the impact of

132 a specific extreme event on the ocean state remains the same in different climates, neglecting

133 possible nonlinearities. Moreover, prescribing SIC poses a particular challenge because the

134 simple addition of a local climate-change signal can lead to unphysical values and, more

135 fundamentally, is not suited for the way sea ice responds to climate change by spatial migration

136 of the ice edge rather than locally continuous changes. Wehrli et al. (2020) addressed this with

137 a rather complex approach, whereas Van Garderen et al. (2021) neglected SIC changes

138 altogether. Given that their focus is on European heatwaves, however, details on how sea ice

139 is treated may not influence their conclusions.

140   The potential of the uncoupled storyline approach in capturing extreme events such as

141 the European heatwaves of 2003 and 2018 along with the Russian heatwave of 2010 has been

142 demonstrated by Wehrli et al. (2020) and Van Garderen et al. (2021). It has been shown, for

143 example, that the fraction of the AgPop region (i.e., latitudes north of 30ºN with a population

144 density above 30 km^{-2} or important for agriculture, as defined by Seneviratne et al. (2018),

145 experiencing daily maximum temperatures higher than 40 ℃ in an event like the 2018

146 heatwave would quadruplicate in a future 4K warmer climate (Wehrli et al. 2020). Van

147 Garderen et al. (2021) found robust warming from preindustrial to present-day for the 2003

148 and 2010 heatwaves, with local warming of about 0–2.5 ℃ (2003) and 0–4 ℃ (2010). In both

149 studies, when the warming is averaged for the heatwave region, an amplified warming

150 (compared to the global-mean warming) is found, except for the 2003 heatwave.

151   The purpose of this work is to further explore and extend the storyline approach using

152 spectral nudging in a coupled model for answering three central questions: First, how would

7

153   the 2019 European summer and particularly the July heatwave have developed in preindustrial

154   times? Second, how might they unfold in future warmer climates (+2 and +4K)? And third, is

155   the coupled storyline approach capable of constraining the surface-ocean and sea-ice states?

156   To this end, we have run experiments with the coupled climate model AWI-CM-1.1-MR

157   (Semmler et al. 2020) with the large-scale atmospheric circulation in the free troposphere being

158   nudged to reanalysis data, while allowing thermodynamic and small-scale dynamical processes

159   to develop relatively freely. Unlike in related previous studies mentioned above, a fully coupled

160   climate model is used that contributed to the sixth phase of the Coupled Model Intercomparison

161   Project (CMIP6; Eyring et al. 2016). By branching the nudging experiments off certain states

162   from the CMIP6 trajectories (e.g., 2K warmer climate), plausible states for the sea ice-ocean

163   component of the climate system are readily available and do not need to be explicitly specified

164   like in corresponding atmosphere-only experiments. In Section 2, we define the methodology

165   used in this work, including the nudging parameters selected. In Section 3, the main results are

166   presented. In Section 4, the obtained results are briefly discussed, and the main conclusions are

167   highlighted.

168

169   **2. Methods**

170   Our simulations are based on the Alfred Wegener Institute Climate Model (AWI-CM-

171   1-1-MR, Semmler et al. 2020). This model has contributed to CMIP6 and employs the

172   atmospheric model ECHAM6.3.04p1 from MPI-M (Stevens et al. 2013) coupled to the Finite

173   Element Sea Ice-Ocean Model (FESOM) v.1.4 (Wang et al. 2014). The atmosphere model is

174   run at T127L95 spectral resolution (~100 km horizontal resolution in the tropics), with 95

175   vertical levels going up to about 0.01 hPa. The ocean mesh has a variable resolution with

176   refinement in energetically active areas such as the Gulf Stream (Sidorenko et al. 2015; Sein et

8

177   al. 2017). More specifically, ocean resolution varies from 8 to 80 km, with 8–10 km used in

178   the North Sea, 10–12 km in the Mediterranean Sea, and 8–20 km in the Arctic (Fig. 1 in

179   Semmler et al. 2020).

180   We have used spectral nudging to impose the observed large-scale circulation for

181   certain atmospheric vertical layers. This technique forces a climate model to follow specific

182   large-scale circulation conditions using reference data from reanalysis (Waldron et al. 1996;

183   Von Storch et al. 2000; Zhang et al. 2014). Spectral nudging is implemented by adding an

184   additional nudging term to the model's governing equations

185
$$\frac{\partial \mathbf{X}_n^m(\eta,t)}{\partial t} = \mathbf{F}_n^m(\eta,t) + \mathbf{G}_n^m(\eta)\left[\mathbf{X}_n^{m(reana)}(\eta,t) - \mathbf{X}_n^m(\eta,t)\right] \tag{1}$$

186   where $\mathbf{X}_n^m(\eta,t)\left(\mathbf{X}_n^{m(reana)}(\eta,t)\right)$ represents the spectral coefficient of a meteorological

187   variable at the vertical level η and timestep t (from the reanalysis), $\mathbf{F}_n^m(\eta,t)$ the model forcing,

188   and $\mathbf{G}_n^m(\eta)$ the nudging coefficient.

189   The impact of nudging depends on which meteorological variables, wavenumbers and

190   vertical levels are constrained. In this work, only divergence and vorticity are nudged. Hence,

191   all other variables can be freely determined by the model. For our main experiments we use a

192   T20 triangular truncation, that is, wavenumbers for vorticity and divergence up to 20 are

193   retained; higher-wavenumber dynamics corresponding to smaller spatial scales can be freely

194   computed by the model. T20 was chosen since this is the lowest total wavenumber for which

195   we found the jetstream (winds at 250 hPa) from ERA5 data (Hersbach et al. 2020) to be

196   qualitatively and quantitatively well constrained (example shown in Fig. 1) when compared to

197   the full field. Furthermore, we chose to only nudge model levels between 100 and 700 hPa.

198   Sensitivity experiments with different vertical profiles of the nudging coefficient have shown

199   that the influence of additionally constraining the stratosphere or lower troposphere is

9

200   negligible (Fig. 2). To avoid overfitting and allow the boundary layer to respond freely,

201   therefore, model levels above 100 hPa and below 700 hPa were not nudged in our simulations.

202   Similar to previous studies (Schubert-Frisius et al. 2017; Wehrli et al. 2018; Van

203   Garderen et al. 2021), a constant nudging strength is used for the constrained levels. To avoid

204   an abrupt transition between neighboring levels, however, the vertical nudging profile has also

205   been smoothed using a sigmoid function (Fig. S1). The nudging strength is related to an e-

206   folding time (τ), with the latter being the inverse of the former (i.e., the larger the e-folding

207   time, the weaker the nudging effect). It turns out that an e-folding time of 24 hours provides a

208   good balance between constraining the large-scale atmospheric circulation and allowing

209   differences depending on the boundary conditions to emerge. Fig. 3 shows 850 hPa winds on

210   one randomly selected day (18 July 2018) from experiments with e-folding times of 6, 24 and

211   48 hours. Results are almost indistinguishable between 6 and 24 hours, with some differences

212   emerging if an e-folding time of 48 hours is used. Hence, 24 hours appears to be a good

213   compromise between imposing the observed atmospheric flow onto the coupled climate model

214   and providing the model with a maximum of freedom to simulate relevant processes and

215   feedbacks, at least for mid-latitude heatwaves considered in this study.

216   With this configuration, we have run nudged storyline experiments using atmospheric

217   forcing fields for the period 1 January 2017 to 30 September 2019. More specifically, nudging

218   experiments with AWI-CM have been branched off the corresponding historical CMIP runs

219   (Semmler et al. 2018) on 1 January 1851 to give *pre-industrial* climate conditions; *present-day*

220   conditions were obtained by branching off the ssp370 scenario (Semmler et al. 2019) on 1

221   January 2017; and 2K and 4K warmer climates were explored by branching off the ssp370

222   scenario on 1 January 2038 and 1 January 2093, respectively (Semmler et al. 2020). For each

223   of the different time slices we have run five ensemble members.

224   The nudged simulations started from different ensemble members of the free-running

225   climate model with different initial states for the atmosphere and ocean. Among others, this

226   allows us to quantify how the different ensemble members adjust to the imposed observed

227   forcing. Fig. 4 shows the temporal evolution of the ensemble spread of European t2m

228   (computed as the difference between the maximum and minimum of all ensemble members for

229   each day) for the nudging experiment under present-day conditions (similar results are obtained

230   for other boundary conditions or variables, not shown). The ensemble spread is larger than 10

231   K at the beginning of the simulations; however, it reduces to about 1.5 K within the first few

232   months, suggesting that the first few months should be discarded from the analysis for

233   atmospheric fields. Nevertheless, we allow for one year of spin-up time to reach a stabilization

234   for more slowly responding parameters such as soil moisture, sea-ice concentration and SST.

235   Accordingly, where not stated otherwise, simulations with the large-scale dynamical conditions

236   for the period 1 January 2018 to 30 September 2019 prescribed for pre-industrial, present-day,

237   and 2K as well as 4K warmer climates are analyzed.

238   Similar to previous studies (e.g., Takhsha et al. 2018; Wehrli et al. 2019), we have

239   found that the global model climatology is not strongly affected by the nudging, with

240   differences within the ensemble spread (not shown). Furthermore, the AWI-CM-1-1-MR free-

241   runs from the CMIP6 archive have been used to compute climatologies (e.g., to determine

242   anomalies and explore weather-dependent amplification of climate change).

243

244   **3. Results**

245   **3.1 Assessment of the nudged simulations for Europe under present-day conditions**

File generated with AMS Word template 1.0

246   Before discussing the storyline scenarios, we compare the present-day nudged

247   simulations with ERA5. Here we focus on Europe; section 3.3 provides an assessment for

248   Arctic sea ice.

249   An example for nudged simulations compared to ERA5 data is given for the 25 July

250   2019 (peak of the heatwave; Fig. 5) before we turn to a quantitative analysis. The anomalous

251   circulation in the coupled climate model on that day, expressed in terms of 500 hPa geopotential

252   height (Z500), is an excellent analogue of the observed blocking conditions. The same is true

253   for parameters such as temperature at 850 hPa (T850) and maximum t2m, which are not directly

254   constrained by the spectral nudging. Overall, the observed characteristics of the heatwave over

255   northwestern Europe are thus well captured. As discussed in more detail below, there is

256   evidence that maximum t2m are slightly underestimated in some regions impacted by the

257   heatwave (Fig. 5e,f). Anomalies of SST and soil moisture at level 1 (SML1) associated with

258   this extreme event are also well captured, confirming that climate anomalies associated with

259   central European heatwaves are strongly driven by atmospheric circulation anomalies. Even

260   fields like total cloud cover (TCC) are reasonably well captured in the Euro-Atlantic region by

261   the nudged simulations for present-day conditions (Fig. 5k,l), suggesting the cloud physical

262   processes are not negatively influenced by the nudging of vorticity and divergence.

263   There are some mismatches between the storyline simulations and ERA5 for this

264   particular day (e.g., in the Balkans, central Iberia and some Arctic regions), noting, however,

265   that for parameters like TCC or SML1 the reanalysis itself is not necessarily well constrained

266   by direct observations. Overall, our results give confidence that the storyline setup with the

267   coupled model captures key processes related to European heatwaves – including atmospheric

268   blocking, warm air advection, clear skies and soil moisture deficits – if driven by large-scale

269   wind fields from ERA5 in the free troposphere.

12

270   So far, our assessment has focused on one particular day at the peak of the July 2019

271   heatwave. For a more comprehensive assessment, correlations between our storyline

272   simulations for present-day conditions and ERA5 as a proxy for observations for the summers

273   of 2018 and 2019 are shown in Fig. 6. Sizeable correlations are obtained for critical variables

274   that are not nudged in our simulations. We have repeated the correlation analysis after having

275   removed low-frequency variability, including the seasonal cycle (i.e., removing a 15-day

276   running mean prior to the analysis). Even for highpass-filtered data, correlations remain high

277   with values exceeding 0.6 for all parameters except soil moisture which is probably more

278   influenced by local convective processes (Fig. S2). In summary, therefore, our methodology

279   does not only work well for single extreme cases; more generally, it also captures daily to

280   seasonal variability in Europe during summertime.

281   This point is further illustrated by Fig. 7, which shows the simulated and reanalyzed

282   maximum, minimum and mean t2m time series for Europe and Germany for the period 1 June

283   to 31 August 2019 (see the definition of these areas in Fig. S3). For both regions, the nudged

284   simulations capture the variability very well. In fact, correlations between simulated and

285   reanalyzed time series mostly exceed r=0.9. For Europe, however, some differences emerge on

286   longer seasonal time scales: While the climate model tends to slightly underestimate t2m in

287   early June, during the course of the summer positive t2m biases emerge. Further analysis

288   suggests that there are small pan-European cold biases in early summer, turning into larger

289   warm biases in southeastern Europe from late June (Fig. S4). The time series for Germany

290   (Fig. 7) generally indicates smaller maximum t2m biases for the coupled model. However,

291   there is some evidence for the exceptionally warm periods in June and July 2019 to be

292   underestimated – especially for maximum t2m during daytime. On the other hand, the coupled

293   model simulates realistic t2m for the third heatwave in late August 2019. Our analysis suggests

294 that the biases are flow-dependent and that there may be even differences between individual

295 extreme events. In this context, it can be argued that the spectral nudging approach – like more

296 sophisticated data assimilation methods such as 4D-Var (e.g., Rodwell and Palmer 2007) – has

297 strong diagnostic potential to help unravel the causes of biases in coupled climate models at

298 the process level, thus guiding model development.

299   To further explore the flow-dependence of the t2m biases for Germany, we have

300 selected the ten days with the strongest positive and strongest negative max t2m differences for

301 Germany between our nudged simulations and ERA5 (Fig. 8), using summer data from 2018

302 and 2019. The most striking finding from this analysis is that the climate model tends to

303 underestimate the maximum t2m during heatwaves in Germany, which are governed by the

304 presence of a pronounced anomalous anticyclonic circulation anomaly, and thus strong

305 European blocking events. No such coherent atmospheric circulation anomaly is found for

306 periods when the simulated t2m in Germany are warmer than in the reanalysis (Fig. 8a,c,e).

307 The finding that the nudged model underestimates extreme t2m during heatwaves in Germany

308 is important, especially when it comes to making quantitative statements on the impact of

309 heatwaves and their future changes.

310

311 **3.2 Storyline scenarios for the European summer of 2019**

312   Having demonstrated that the spectral nudging approach with the coupled climate

313 model works well, we now analyze how the summer of 2019, including the July heatwave,

314 might have evolved in pre-industrial times and how it might unfold in future 2K and 4K warmer

315 climates. For Germany, there is very robust warming for maximum and minimum t2m (i.e., the

316 ensembles for different climates do not overlap) that tends to grow throughout the summer

317 season – from pre-industrial times to the present and from present-day to 4K warmer climates

14

318 (Fig. 9). Changes in maximum and minimum t2m from present-day conditions (approximately

319 +1.2K in the storyline experiments) to a 2K warmer climate are smaller, even though they are

320 still quite robust in terms of the separation of the two ensembles. In general, these findings are

321 consistent with the free-running CMIP6 simulations (dashed lines in Fig. 9), suggesting that

322 they are not a particular feature of this specific summer.

323   Another point illustrated by Fig. 9 is that in nighttime t2m (minimum t2m) in Germany

324 in a 4K warmer world are projected to become comparable to typical daytime maxima

325 (maximum t2m) in pre-industrial times – at least for the heatwaves that occurred in late July

326 and August 2019.

327   Remarkably, this anthropogenic warming in Germany has an intraseasonal cycle (Fig.

328 S5 for maximum t2m with similar results for minimum t2m, not shown), with values close to

329 the global average in early summer, and increasing relative to global value in mid and late

330 summer. In fact, values around +5.5 K (+4K minus present-day), +0.8 K (+2K minus present-

331 day) and +2.0 K (present-day minus pre-industrial) are obtained for the July heatwave peak.

332 Hence, there is evidence for global warming amplification in phase with the July event,

333 particularly in the 4K warmer climate (2-fold increase). Similar results can be found in the free

334 run, so this amplification is not specific to the events in July 2019. When the differences are

335 computed for +2K minus pre-industrial and +4K minus +2K, then non-significantly higher

336 warming is obtained for the latter (Fig. S5, bottom). This suggests that there might be some

337 feedback mechanisms generating a slightly higher than expected warming in the future.

338   The European heatwaves during the summer of 2019 did not only impact land areas;

339 they were also accompanied by ocean heatwaves in the North Sea, as demonstrated in Fig. 10,

340 which shows the evolution of SST in the North Sea and the German Bight (see their definition

341 in Fig. S3). Generally, the ocean heatwaves are more pronounced for the latter region. This is

15

342   not too surprising given that it represents a smaller and shallow area that lies closer to the area

343   most impacted by the heatwaves. Around mid-July, SST in the German Bight is about 1 K

344   cooler in the nudged runs compared to the climatological signal derived from the free runs;

345   shortly before the 25 July, anomalies turn positive, reaching about +2 K in late July and early

346   August. Thus, the impact of heatwaves on SST in both areas suggests that using coupled

347   climate models for storyline scenarios may be an advantage when it comes to capturing events

348   that are impacted by coupled processes.

349   From a climatological point of view, the warming of SST in the German Bight from

350   pre-industrial times to the 4K warmer world amounts to about 4 K. This is quite a substantial

351   change compared to SST changes in the open ocean (~3 K). The ocean heatwave in early

352   August, for example, would have been accompanied by SSTs of about 20 ºC in pre-industrial

353   times; in a 4K warmer world SSTs could reach up to 24 ºC. The change is probably even larger

354   in the shallow waters closer to the coast not resolved by the climate model (~8 km is used in

355   the North Sea). Furthermore, it is worth pointing out that, compared to t2m, for SST changes

356   there is even less evidence for a warming acceleration when comparing the warming from +2K

357   to +4K against the warming from pre-industrial times to +2K (Fig. A6). This is consistent with

358   an earlier finding that the observed warming in the North Sea during the last few decades was

359   quite strong (Wiltshire et al. 2010).

360   The evolution of SST warming in the nudged 2019 storyline simulations exhibits some

361   interesting differences compared to the corresponding climatological warming. For example,

362   considering the change from present-day to the 4K warmer climate, SSTs in the German Bight

363   increase by about 0.5 K more in the storyline runs in June 2019 compared to the climatological

364   warming, whereas the opposite holds for August 2019 (Fig. S6), resulting in a dampened

365   strength of the late-summer heatwaves (Fig. 10). This provides evidence for a dependence of

16

366 the SST climate-change signal on weather patterns which could not be captured by storyline

367 scenarios using atmospheric models with prescribed SSTs.

368   Spatial maps of the t2m differences on 25 July 2019 between the different climates for

369 the wider European region are shown in Fig. 11. These maps describe the "warming signal of

370 the day", given the large-scale circulation and its evolution during the preceding days, weeks

371 and months. Some well-known climate change features (e.g., Fischer and Schär 2010;

372 Barcikowska et al. 2020; Suarez-Gutierrez et al. 2020) emerge for this particular day: For

373 example, extreme temperatures over land areas tend to increase more strongly than those over

374 the ocean; the warming is more pronounced in southern Europe compared to more northern

375 regions of continental Europe; and the warming signal tends to move northward during the 21st

376 century. Furthermore, anomalously strong warming signals can be found locally in some of the

377 regions (e.g., northeastern Spain and southwestern France), which supports the notion that there

378 may be some "weather-dependent amplification" of climate change. However, not all of the

379 small-scale structures may be due to this weather dependence. Some of the differences may

380 simply be "random", for example depending on the presence of clouds (less well constrained

381 and thus more uncertain) and hence the strength of the incoming solar radiation.

382   From Fig. 11 it can also be inferred that for some regions in Germany, the additional

383 warming from present-day conditions to the end of the 21st century (4K warmer world) would

384 amount to as much as 7 K. By adding the 3.6 K experienced today compared to pre-industrial

385 times, locally maximum t2m by the end of the century could exceed 47 ℃; in contrast,

386 maximum t2m would have stayed below 37 ℃ in pre-industrial times – certainly extreme, but

387 not necessarily dangerously high (see Fig. 18 in the Discussion and conclusions section).

388   We have also explored the connection between changes in t2m, soil wetness and Bowen

389 ratio, which is defined as the ratio of sensible to latent heat fluxes. The seasonal evolution of

17

390   soil wetness and the Bowen ratio in the different climates is shown in Fig. 12. The summer of

391   2019 starts with anomalously dry soils that were comparable for the different climates (i.e., the

392   ensembles show some overlap). Furthermore, latent heat flux dominates over sensible heat flux

393   in June, as indicated by the Bowen ratios remaining below 0.5 for all climates. Driven by the

394   first heatwave in late June 2019 (Fig. 9), a dramatic decrease in soil wetness is witnessed in all

395   simulations, with values reaching the 5th quantile obtained from the CMIP6 (dotted lines in

396   Fig. 12). The more moderate conditions in early and mid-July led to a minor increase in soil

397   wetness. As a consequence, the July heatwave occurred with anomalously, but not

398   exceptionally dry soils (below the 4K warmer climate climatology). In early July, the reduced

399   soil moisture availability triggered an increase in Bowen ratio to values around 1. Nevertheless,

400   after a small decrease in mid-July, the values on the heatwave peak are only slightly higher

401   than the climatology. This suggests that dry soils exacerbated the July heatwave but were not

402   a key factor.

403   Remarkably, the consequences of the June event in both variables are even greater in

404   the 4K warmer climate, with robustly drier conditions and a higher Bowen ratio from early July

405   to the end of the season. Thus, these higher changes in the radiative fluxes (due to a lack of soil

406   moisture) can partly explain the larger warming amplification observed in this area in the future

407   4K warmer climate. Therefore, a heatwave in early summer (as in 2003 or 2019) could

408   exacerbate a heatwave occurring later (high summer) as it creates dry soil conditions that

409   intensify the second event by changes in the surface heat fluxes. Furthermore, at least for the

410   2019 summer, this effect would be stronger in the 4K warmer climate than in the preindustrial

411   to 2K warmer climates.

412   Maps of soil wetness and Bowen ratio for 25 July 2019 are shown in Fig. 13. They help

413   to explain the global warming amplification and non-linear changes found for t2m. From the

18

414   pre-industrial to present-day climates, there is a strong and robust drying in the Mediterranean

415   region which is accompanied by a dramatic increase in Bowen Ratio. Meanwhile, in central

416   and northern Europe differences are relatively small due to the availability of sufficient soil

417   moisture. When considering future changes (i.e., +4K minus present-day) the drying of the soil

418   and the increase in Bowen ratio peak in mid-latitude regions, including central Europe

419   .

420   **3.3 Storyline scenarios for Arctic sea ice**

421   The use of a coupled model allows studying coupled environmental extreme events, as

422   mentioned in Section 3.2 for SST in the North Sea. Here we provide some initial insight into

423   the value of the coupled storyline scenario approach for Arctic sea ice. In general, studying

424   sea-ice anomalies in a coupled storyline approach might be useful not only to explore more

425   directly sea-ice related extremes, such as the opening of polynyas north of Greenland (Moore

426   et al. 2018; Ludwig et al. 2019); sea-ice anomalies have also been shown to influence mid-

427   latitude events, such as extreme snowfall in northern Europe, through modification of air

428   masses (Bailey et al. 2021). Here we therefore briefly discuss how Arctic sea-ice anomalies

429   and changes are represented in our coupled storyline simulations, acknowledging that sea ice

430   probably had a minor role to play when it comes to thermodynamic processes driving European

431   heatwaves.

432   Daily anomalies of the pan-Arctic sea-ice extent (area with SIC > 15%) are relatively

433   coherent between the nudged simulation and ERA5 (Fig. 14). Omitting the first year, where

434   the model state might still be affected by the spin-up, the Pearson correlation for the ensemble

435   mean is ~0.65 (~0.53 if the first year is included). While some of the strong anomalies are

436   clearly captured, in particular during the second half of 2018, some anomalies are not well

437   captured by the nudged simulation. In particular, observed negative anomalies around April

19

438 both in 2018 and 2019 are in contrast to positive anomalies in the storyline simulations.

439 However, it is worth noting that the ensemble spread during these inconsistent periods is much

440 larger than during the second half of 2018, suggesting that the sea-ice state may be less strongly

441 constrained by the large-scale circulation in the early melt season compared to other times of

442 the year.

443   Another factor that can lead to inconsistent anomalies is model bias. While this

444 probably holds for any quantity, it may be particularly influential for the sea-ice state. Moderate

445 temperature biases, for example, can lead to significant errors in the ice-edge location. As a

446 consequence, the ice-edge location in a biased model will respond differently to the same large-

447 scale circulation anomaly pattern, simply because the ice edge resides in a different place.

448 Indeed, AWI-CM free runs exhibit non-negligible biases in the ice-edge location (Semmler et

449 al. 2020), and nudging only the large-scale dynamics does not – and is not meant to – rectify

450 thermodynamically-induced model biases. In July, for example, the climatological ice edge

451 extends much further into the Barents and Kara Seas in AWI-CM compared to ERA5 (black

452 contours in Fig. 15). However, despite these limitations, the regional patterns of sea-ice

453 concentration anomalies tend to be captured rather well. For example, during the Arctic melt

454 season 2019 on 25 July (the peak of the central European heatwave), negative SIC anomalies

455 prevailed in the Chukchi, East Siberian, and Laptev Seas, whereas positive anomalies prevailed

456 in (or north of) the Barents and Beaufort Seas (Fig. 15, bottom). While the moderately negative

457 pan-Arctic sea-ice extent anomaly at that time is not reproduced (the simulated anomalies are

458 near-neutral; Fig. 14), the spatial patterns are reasonably well captured (Fig. 15, top).

459   The fact that the ice edge responds differently to large-scale circulation anomalies

460 depending on where it resides on average is even more important when it comes to sea-ice

461 anomalies in significantly different climates: The climatological sea-ice distributions in the

462　pre-industrial, present, +2K, and +4K climates are vastly different (Fig. 16). For example, one

463　cannot expect that a large-scale circulation pattern that causes, or at least contributes to, a

464　record-low pan-Arctic sea-ice extent in pre-industrial or present climate would have a similar

465　effect in a 4K warmer climate, where scarcely any Arctic sea ice remains even in July (Fig.

466　16), two months before the end of the classical melt season. This may complicate the

467　assessment to what extent sea-ice anomalies associated with a specific extreme event may

468　amplify or dampen some aspects of the event when transferred to a different climate. However,

469　as it is the case for SSTs, it is arguably more physically consistent regarding the two-way

470　interaction of sea ice with an extreme event to simulate the sea-ice response in a coupled model

471　rather than to prescribe the sea-ice state and its response in some non-trivial way.

472

473　**4. Discussion and Conclusions**

474　　In this study we present a method for computing storyline scenarios using spectral

475　nudging in a coupled climate model. The strength of this approach lies in the use of a coupled

476　climate model that has contributed to CMIP6 (i.e., AWI-CM-1-1-MR, Semmler et al. 2020).

477　By using a coupled approach one can study climate and environmental extremes in a coupled

478　framework, thereby avoiding possible shortcomings that arise from having to specify SST and

479　sea-ice conditions for past and future climates. In this context, the availability of CMIP6

480　simulations, from which the nudging experiments can be branched off, is a distinct advantage.

481　By applying a scale-dependent, spectral nudging approach in the free troposphere only, as in

482　Van Garderen et al. (2021), it is possible to constrain only the large-scale circulation associated

483　with the jet stream, which is known to be one of the key drivers of extreme and high-impact

484　environmental events in mid-latitudes.

485   The full potential of this approach can further be inferred from Fig. 17, illustrating

486   coupled storyline scenarios for 1600 UTC 20 September 2019 – another event in late

487   summer/early autumn 2019. This confirms that (i) the jet stream, i.e., the dynamically driver,

488   is realistically represented; (ii) anthropogenic warming is strongest over land, especially when

489   considering changes from present-day condition to a 4K warmer world; (iii) locally extreme

490   SSTs anomalies (i.e., ocean heatwaves) emerge in the Mediterranean Sea, with SSTs

491   exceeding +30 ºC in the central Mediterranean Sea; and (iv) there are vastly different sea-ice

492   conditions in the Arctic that are consistent with the atmospheric state and its previous evolution.

493   We should note that the last two points are treated in a physically more consistent way in

494   coupled storyline scenarios than it could by prescribing SST and SIC fields in atmosphere-only

495   storyline scenarios.

496   The storyline approach, employing nudging, is computationally quite efficient, at least

497   once CMIP-type simulations are available from which nudged simulations can be branched off.

498   This is due to the fact that the main source of uncertainty in future projections of European

499   extreme events – that is strong internal atmospheric variability compared to relatively weak

500   climate change signals – has been effectively "removed" by prescribing the temporal evolution

501   of the large-scale mid-troposphere dynamics. In fact, in agreement with Wehrli et al. (2020)

502   and Van Garderen et al. (2021), for European heatwaves just a few ensemble members are

503   sufficient to separate signal from noise, once the evolution of the large-scale atmospheric

504   circulation is prescribed.

505   As pointed out by Shepherd et al. (2018), storyline scenarios provide a very effective

506   way of making the impacts of climate change more tangible to experts and non-experts alike

507   – thus facilitating decision-making in adaptation and mitigation. This point is further illustrated

508   in Fig. 18, showing "weather maps" of t2m during the peak of this record-breaking heatwave

22

509   in Germany in July 2019 for present-day, pre-industrial and future conditions: While this

510   weather event was clearly extreme by nature, with maximum t2m of about 37 ℃ even without

511   anthropogenic warming, the warming since pre-industrial times made it record-breaking (42

512   ℃ in places) with substantial impacts on society, businesses and infrastructure, including a

513   "meltdown" of the German railway system. In a 4K warmer world (i.e., 3 K warmer than today)

514   daytime t2m would be reaching dangerously high values, nearing 50 ℃. The value of this

515   approach for understanding and communicating the impact of climate change could be further

516   enhanced by using these storyline scenarios to drive impact models. In this way, it would

517   become possible to draw more complete "pictures", for example by also making statements

518   about surface hydrology, river levels and the state of the vegetation.

519   It seems likely that finding analogs of similar quality from observations, CMIP data

520   and large ensembles will be difficult, if possible at all. This is especially true if the temporal

521   dimension is taken into account, which is critical when it comes to parameters such as soil

522   moisture and SST that memorize past weather and are not only of interest in their own right

523   but also feedback on temperatures during the evolution of heatwaves.

524   The coupled storyline approach, presented in this study, also provides a very powerful

525   way of diagnosing the origin of model error at the process level, thus guiding future model

526   development. Usually, one of the main challenges in diagnosing coupled models arises from

527   the fact that a direct comparison with observations from field campaigns, which are usually

528   comprehensive and of high quality but limited in time, is difficult to carry out. Therefore,

529   disentangling differences due to different weather from those due to model deficiencies

530   becomes difficult. Recognizing this, activities such as Transpose-CMIP – that is, running short-

531   term predictions with initialized coupled climate models – have been proposed and applied

532   (e.g., Voldoire et al. 2019). Here we argue that the storyline simulations, using spectral nudging

23

533　in climate models, provide another promising way of analyzing model shortcomings, including

534　those that occur only sporadically during certain weather types (i.e., flow-dependent biases).

535　To explore this idea further, we are planning to extend the experiments until the end of 2020

536　and provide a thorough comparison with observational data from the MOSAiC expedition –

537　the year-round drift through the Arctic which lasted from October 2019 to October 2020.

538　Related to this, the approach proposed in this study provides a powerful technique to

539　understand and quantify how coupled processes associated with certain phenomena (e.g.,

540　heatwaves, sea-ice polynyas and cold-air outbreaks) change in different climates. The fact that

541　dry soils in southern Europe at the end of the 21st century in a 4K warmer world are projected

542　to change the role of how the atmosphere interacts with the soil is a promising example.

543　　　Storyline scenarios are in principle not limited to specific types of events. However, it

544　is likely not a coincidence that studies demonstrating the approach so far have been focussing

545　on heatwaves; these have a rather large-scale footprint and can thus be reproduced relatively

546　easily by constraining the large-scale dynamics. While the same may hold for cold-extremes

547　in winter, events that occur on smaller scales and involve small-scale dynamics and fronts,

548　including extreme rainfall events like the devastating flash floods in western Germany in July

549　2021, are more challenging. In our setup, where the nudging is relatively weak and leaves

550　wavenumbers above 20 free, extreme rains are clearly underestimated (not shown). Dedicated

551　efforts are needed to extend the storyline approach to different types of events. It is possible

552　that different event types will require different optimal settings, and that events with a strong

553　small-scale random component may necessitate a large-ensemble storyline approach.

554　　　To summarize, this work presents the first storyline of the European July 2019

555　heatwave augmenting previous probabilistic attribution studies (Ma et al. 2020; Vautard et al.

556　2020) in which changes of the frequency of occurrence of certain events in different climates

File generated with AMS Word template 1.0

557 are quantified. The most outstanding finding of this study is the global warming amplification

558 found associated with the July 2019 heatwave (locally up to 4-fold increase). This

559 amplification is enhanced and northward displaced in the future 4K warmer climate, with more

560 than a 2-fold increase in Germany (both for maximum and minimum t2m). In contrast with the

561 result obtained by Van Garderen et al. (2021) for the European 2003 heatwave, an amplification

562 is also found from preindustrial to present climate (an ~1.5-fold increase in Germany), with the

563 highest warming found in the Mediterranean region. The warming obtained for the 2019

564 summer is similar to the climatological mean warming, as may be due to a climatological

565 drying of soils comparable to the drying that occurred during the 2019 summer. In addition,

566 we have not found significant flow-dependent stronger or weaker changes in our simulations

567 (not shown). However, this last result should be assessed using simulations that span longer

568 periods, e.g., starting in 1979. Meanwhile, neither a future global warming amplification nor a

569 summer intraseasonal cycle of warming is found for SST in our study areas, more specifically,

570 the North Sea. However, the observed SST warming there is close to the global warming and

571 thus stronger than the mean ocean-surface warming.

572   Overall, our study adds further support to the notion that storyline scenarios provide a

573 promising approach that augments traditional probabilistic approaches to the attribution of

574 extreme events and that help to make climate change and its impact more tangible to scientists,

575 decision-makers and the general public.

576

File generated with AMS Word template 1.0

585 *Data Availability Statement.*

592

593

594

595

596

597

598

599

600

601

602

REFERENCES

Bador, M., L. Terray, J. Boé, S. Somot, A. Alias, A. L. Gibelin, and B. Dubuisson, 2017: Future summer mega-heatwave and record-breaking temperatures in a warmer France climate. *Environ. Res. Lett.*, **12**, 074025, https://doi.org/10.1088/1748-9326/aa751c.

Bailey, H., A. Hubbard, E. S. Klein, K.-R. Mustonen, P. D. Akers, H. Marttila, and J. M. Welker, 2021: Arctic sea-ice loss fuels extreme European snowfall. *Nat. Geosci.*, **14**, 283–288, https://doi.org/10.1038/s41561-021-00719-y.

Barbi, D., N. Wieters, P. Gierz, M. Andrés-Martínez, D. Ural, F. Chegini, S. Khosravi, and L. Cristini, 2021: ESM-Tools version 5.0: a modular infrastructure for stand-alone and coupled Earth system modelling (ESM). *Geosci. Model Dev.*, **14**, 4051–4067, https://doi.org/10.5194/gmd-14-4051-2021.

Barcikowska, M. J., S. B. Kapnick, L. Krishnamurty, S. Russo, A. Cherchi, and C. K. Folland, 2020: Changes in the future summer Mediterranean climate: contribution of teleconnections and local factors. *Earth Syst. Dyn.*, **11**, 161–181, https://doi.org/10.5194/esd-11-161-2020.

Barriopedro, D., E. M. Fischer, J. Luterbacher, R. M. Trigo, and R. García-Herrera, 2011: The Hot Summer of 2010: Redrawing the Temperature Record Map of Europe. *Science*, **332**, 220–224, https://doi.org/10.1126/science.1201224.

Beillouin, D., B. Schauberger, A. Bastos, P. Ciais, and D. Makowski, 2020: Impact of extreme weather conditions on European crop production in 2018. *Philos. Trans. Roy. Soc. B Biol. Sci.*, **375**, 20190510, https://doi.org/10.1098/rstb.2019.0510.

27

624   Cattiaux, J., H. Douville, R. Schoetter, S. Parey, and P. Yiou, 2015: Projected increase in

625   diurnal and interdiurnal variations of European summer temperatures. *Geophys. Res. Lett.*,

626   **42**, 899–907, https://doi.org/10.1002/2014GL062531.

627   Centre for research on the epidemiology of disasters (CRED), 2020: Natural disasters 2019:

628   Now is the time to not give up, 8pp, https://cred.be/sites/default/files/adsr_2019.pdf.

629   Chapman, S. C., N. W. Watkins, and D. A. Stainforth, 2019: Warming Trends in Summer

630   Heatwaves. *Geophys. Res. Lett.*, **46**, 1634–1640, https://doi.org/10.1029/2018GL081004.

631   Della-Marta, P. M., M. R. Haylock, J. Luterbacher, and H. Wanner, 2007: Doubled length of

632   western European summer heat waves since 1880. *J. Geophys. Res: Atmospheres*, **112**,

633   D15103, https://doi.org/10.1029/2007JD008510.

634   Dole, R., and Coauthors, 2011: Was there a basis for anticipating the 2010 Russian heat wave?

635   *Geophys. Res. Lett.*, **38**, L06702, https://doi.org/10.1029/2010GL046582.

636   Dommenget, D., 2009: The Ocean's Role in Continental Climate Variability and Change. *J.*

637   *Climate*, **22**, 4939–4952, https://doi.org/10.1175/2009JCLI2778.1.

638   Duchez, A., and Coauthors, 2016: Drivers of exceptionally cold North Atlantic Ocean

639   temperatures and their link to the 2015 European heat wave. *Environ. Res. Lett.*, **11**,

640   074004, https://doi.org/10.1088/1748-9326/11/7/074004.

641   Eyring, V., S. Bony, G. A. Meehl, C. A. Senior, B. Stevens, R. J. Stouffer, and K. E. Taylor,

642   2016: Overview of the Coupled Model Intercomparison Project Phase 6 (CMIP6)

643   experimental design and organization. *Geosci. Model Dev.*, **9**, 1937–1958,

644   https://doi.org/10.5194/gmd-9-1937-2016.

645 Fan, X., Q. Duan, C. Shen, Y. Wu, and C. Xing, 2020: Global surface air temperatures in

646   CMIP6: historical performance and future changes. *Environ. Res. Lett.*, **15**, 104056,

647   https://doi.org/10.1088/1748-9326/abb051.

648 Fischer, E. M., and C. Schär, 2010: Consistent geographical patterns of changes in high-impact

649   European heatwaves. *Nat. Geosci.*, **3**, 398–403, https://doi.org/10.1038/ngeo866.

650 Garrido-Perez, J. M., C. Ordóñez, R. García-Herrera, and J. L. Schnell, 2019: The differing

651   impact of air stagnation on summer ozone across Europe. *Atmos. Environ.*, **219**, 117062,

652   https://doi.org/10.1016/j.atmosenv.2019.117062.

653 Hersbach, H., and Coauthors, 2020: The ERA5 global reanalysis. *Quart. J. Roy. Meteor. Soc.*,

654   **146**, 1999–2049, https://doi.org/10.1002/qj.3803.

655 Hoskins, B., and T. Woollings, 2015: Persistent Extratropical Regimes and Climate Extremes.

656   *Curr. Climate Change Rep.*, **1**, 115–124, https://doi.org/10.1007/s40641-015-0020-8.

657 IPCC, 2018: Global Warming of 1.5°C. An IPCC Special Report on the impacts of global

658   warming of 1.5°C above pre-industrial levels and related global greenhouse gas emission

659   pathways, in the context of strengthening the global response to the threat of climate

660   change, sustainable development, and efforts to eradicate poverty, V.Masson-Delmotte et

661   al., Eds.. 630 pp,

662   https://www.ipcc.ch/site/assets/uploads/sites/2/2019/06/SR15_Full_Report_High_Res.pdf

663 Jézéquel, A., P. Yiou, and S. Radanovics, 2018: Role of circulation in European heatwaves

664   using flow analogues. *Climate Dyn.*, **50**, 1145–1159, https://doi.org/10.1007/s00382-017-

665   3667-0.

Junk, J., K. Goergen, and A. Krein, 2019: Future Heat Waves in Different European Capitals Based on Climate Change Indicators. *Int. J. Environ. Res. Public. Health*, **16**, 3959, https://doi.org/10.3390/ijerph16203959.

Konovalov, I. B., M. Beekmann, I. N. Kuznetsova, A. Yurova, and A. M. Zvyagintsev, 2011: Atmospheric impacts of the 2010 Russian wildfires: integrating modelling and measurements of an extreme air pollution episode in the Moscow region. *Atmos. Chem. Phys.*, **11**, 10031–10056, https://doi.org/10.5194/acp-11-10031-2011.

Lesk, C., P. Rowhani, and N. Ramankutty, 2016: Influence of extreme weather disasters on global crop production. *Nature*, **529**, 84–87, https://doi.org/10.1038/nature16467.

Ludwig, V., G. Spreen, C. Haas, L. Istomina, F. Kauker, and D. Murashkin, 2019: The 2018 North Greenland polynya observed by a newly introduced merged optical and passive microwave sea-ice concentration dataset. *Cryosphere*, **13**, 2051–2073, https://doi.org/10.5194/tc-13-2051-2019.

Ma, F., X. Yuan, Y. Jiao, and P. Ji, 2020: Unprecedented Europe Heat in June–July 2019: Risk in the Historical and Future Context. *Geophys. Res. Lett.*, **47**, e2020GL087809, https://doi.org/10.1029/2020GL087809.

Madruga De Brito, M., C. Kuhlicke, and A. Marx, 2020: Near-real-time drought impact assessment: a text mining approach on the 2018/19 drought in Germany. *Environ. Res. Lett.*, **15**, 1040a9, https://doi.org/10.1088/1748-9326/aba4ca.

Miralles, D. G., P. Gentine, S. I. Seneviratne, and A. J. Teuling, 2019: Land–atmospheric feedbacks during droughts and heatwaves: state of the science and current challenges. *Ann. N. Y. Acad. Sci.*, **1436**, 19–35, https://doi.org/10.1111/nyas.13912.

688 Mitchell, D., K. Kornhuber, C. Huntingford, and P. Uhe, 2019: The day the 2003 European

689 heatwave record was broken. *Lancet Planet. Health*, **3**, e290–e292,

690 https://doi.org/10.1016/S2542-5196(19)30106-8.

691 Moore, G. W. K., A. Schweiger, J. Zhang, and M. Steele, 2018: What Caused the Remarkable

692 February 2018 North Greenland Polynya? *Geophys. Res. Lett.*, **45**, 13,342-13,350,

693 https://doi.org/10.1029/2018GL080902.

694 Perkins-Kirkpatrick, S. E., and S. C. Lewis, 2020: Increasing trends in regional heatwaves. *Nat.*

695 *Commun.*, **11**, 1–8, https://doi.org/10.1038/s41467-020-16970-7.

696 Rodwell, M. J., and T. N. Palmer, 2007: Using numerical weather prediction to assess climate

697 models. *Quart. J. Roy. Meteor. Soc.*, **133**, 129–146, https://doi.org/10.1002/qj.23.

698 Russo, S., J. Sillmann, and E. M. Fischer, 2015: Top ten European heatwaves since 1950 and

699 their occurrence in the coming decades. *Environ. Res. Lett.*, **10**, 124003,

700 https://doi.org/10.1088/1748-9326/10/12/124003.

701 Sánchez-Benítez, A., R. García-Herrera, D. Barriopedro, P. M. Sousa, and R. M. Trigo, 2018:

702 June 2017: The Earliest European Summer Mega-heatwave of Reanalysis Period. *Geophys.*

703 *Res. Lett.*, **45**, 1955–1962, https://doi.org/10.1002/2018GL077253.

704 ——, D. Barriopedro, and R. García-Herrera, 2020: Tracking Iberian heatwaves from a new

705 perspective. *Wea. Climate Extrem.*, **28**, 100238,

706 https://doi.org/10.1016/j.wace.2019.100238.

707 Schoetter, R., J. Cattiaux, and H. Douville, 2015: Changes of western European heat wave

708 characteristics projected by the CMIP5 ensemble. *Climate Dyn.*, **45**, 1601–1616,

709 https://doi.org/10.1007/s00382-014-2434-8.

710 Schubert-Frisius, M., F. Feser, H. von Storch, and S. Rast, 2017: Optimal spectral nudging for

711 global dynamic downscaling. *Mon. Wea. Rev.*, **145**, 909–927,

712 https://doi.org/10.1175/MWR-D-16-0036.1.

713 Sein, D. V., and Coauthors, 2017: Ocean Modeling on a Mesh With Resolution Following the

714 Local Rossby Radius. *J. Adv. Model. Earth Syst.*, **9**, 2601–2614,

715 https://doi.org/10.1002/2017MS001099.

716 Semmler, T., and Coauthors, 2018: AWI AWI-CM1.1MR model output prepared for CMIP6

717 CMIP historical. https://doi.org/10.22033/ESGF/CMIP6.2686.

718 ——, and Coauthors, 2019: AWI AWI-CM1.1MR model output prepared for CMIP6

719 ScenarioMIP ssp370. https://doi.org/10.22033/ESGF/CMIP6.2803.

720 ——, and Coauthors, 2020: Simulations for CMIP6 With the AWI Climate Model AWI-CM-

721 1-1. *J. Adv. Model. Earth Syst.*, **12**, 1–34, https://doi.org/10.1029/2019MS002009.

722 Seneviratne, S. I., and Coauthors, 2018: Land radiative management as contributor to regional-

723 scale climate adaptation and mitigation. *Nat. Geosci.*, **11**, 88–96,

724 https://doi.org/10.1038/s41561-017-0057-5.

725 Shepherd, T. G., 2014: Atmospheric circulation as a source of uncertainty in climate change

726 projections. *Nat. Geosci.*, **7**, 703–708, https://doi.org/10.1038/NGEO2253.

727 ——, 2016: A Common Framework for Approaches to Extreme Event Attribution. *Curr.*

728 *Climate Change Rep.*, **2**, 28–38, https://doi.org/10.1007/s40641-016-0033-y.

729 ——, and Coauthors, 2018: Storylines: an alternative approach to representing uncertainty in physical aspects of climate change. *Climate Change*, **151**, 555–571, https://doi.org/10.1007/s10584-018-2317-9.

732 Sidorenko, D., and Coauthors, 2015: Towards multi-resolution global climate modeling with ECHAM6–FESOM. Part I: model formulation and mean climate. *Climate Dyn.*, **44**, 757–780, https://doi.org/10.1007/s00382-014-2290-6.

735 Sousa, P. M., D. Barriopedro, R. García-Herrera, C. Ordóñez, P. M. M. Soares, and R. M. Trigo, 2020: Distinct influences of large-scale circulation and regional feedbacks in two exceptional 2019 European heatwaves. *Commun. Earth Environ.*, **1**, 48, https://doi.org/10.1038/s43247-020-00048-9.

739 Stevens, B., and Coauthors, 2013: Atmospheric component of the MPI-M earth system model: ECHAM6. *J. Adv. Model. Earth Syst.*, **5**, 146–172, https://doi.org/10.1002/jame.20015.

741 Suarez-Gutierrez, L., W. A. Müller, C. Li, and J. Marotzke, 2020: Dynamical and thermodynamical drivers of variability in European summer heat extremes. *Climate Dyn.*, **54**, 4351–4366, https://doi.org/10.1007/s00382-020-05233-2.

744 Sutanto, S. J., C. Vitolo, C. Di Napoli, M. D'Andrea, and H. A. J. Van Lanen, 2020: Heatwaves, droughts, and fires: Exploring compound and cascading dry hazards at the pan-European scale. *Environ. Int.*, **134**, 105276, https://doi.org/10.1016/j.envint.2019.105276.

747 Takhsha, M., O. Nikiéma, P. Lucas-Picher, R. Laprise, L. Hernández-Díaz, and K. Winger, 2018: Dynamical downscaling with the fifth-generation Canadian regional climate model (CRCM5) over the CORDEX Arctic domain: effect of large-scale spectral nudging and of

33

750   empirical correction of sea-surface temperature. *Climate. Dyn.*, **51**, 161–186,

751   https://doi.org/10.1007/s00382-017-3912-6.

752   Trigo, R. M., R. García-Herrera, J. Díaz, I. F. Trigo, and M. A. Valente, 2005: How exceptional

753   was the early August 2003 heatwave in France? *Geophys. Res. Lett.*, **32**, L10701,

754   https://doi.org/10.1029/2005GL022410.

755   van der Wiel, K., F. M. Selten, R. Bintanja, R. Blackport, and J. A. Screen, 2020: Ensemble

756   climate-impact modelling: extreme impacts from moderate meteorological conditions.

757   *Environ. Res. Lett.*, **15**, 034050, https://doi.org/10.1088/1748-9326/ab7668.

758   Van Garderen, L., F. Feser, and T. G. Shepherd, 2021: A methodology for attributing the role

759   of climate change in extreme events: A global spectrally nudged storyline. *Nat. Hazards*

760   *Earth Syst. Sci.*, **21**, 171–186, https://doi.org/10.5194/nhess-21-171-2021.

761   Vautard, R., and Coauthors, 2020: Human contribution to the record-breaking June and July

762   2019 heatwaves in Western Europe. *Environ. Res. Lett.*, **15**, https://doi.org/10.1088/1748-

763   9326/aba3d4.

764   Vogel, M. M., R. Orth, F. Cheruy, S. Hagemann, R. Lorenz, B. J. J. M. van den Hurk, and S.

765   I. Seneviratne, 2017: Regional amplification of projected changes in extreme temperatures

766   strongly controlled by soil moisture-temperature feedbacks. *Geophys. Res. Lett.*, **44**, 1511–

767   1519, https://doi.org/10.1002/2016GL071235.

768   ——, J. Zscheischler, R. Wartenburger, D. Dee, and S. I. Seneviratne, 2019: Concurrent 2018

769   Hot Extremes Across Northern Hemisphere Due to Human-Induced Climate Change.

770   *Earths Future*, **7**, 692–703, https://doi.org/10.1029/2019EF001189.

771   Voldoire, A., and Coauthors, 2019: Evaluation of CMIP6 DECK Experiments With CNRM-

772   CM6-1. *J. Adv. Model. Earth Syst.*, **11**, 2177–2213,

773   https://doi.org/10.1029/2019MS001683.

774   Von Storch, H., H. Langenberg, and F. Feser, 2000: A spectral nudging technique for

775   dynamical downscaling purposes. *Mon. Wea. Rev.*, **128**, 3664–3673,

776   https://doi.org/10.1175/1520-0493(2000)128<3664:ASNTFD>2.0.CO;2.

777   Waldron, Kim. M., J. Paegle, and J. D. Horel, 1996: Sensitivity of a Spectrally Filtered and

778   Nudged Limited-Area Model to Outer Model Options. *Mon. Wea. Rev.*, **124**, 529–547,

779   https://doi.org/10.1175/1520-0493(1996)124<0529:SOASFA>2.0.CO;2.

780   Wang, Q., S. Danilov, D. Sidorenko, R. Timmermann, C. Wekerle, X. Wang, T. Jung, and J.

781   Schröter, 2014: The Finite Element Sea Ice-Ocean Model (FESOM) v.1.4: Formulation of

782   an ocean general circulation model. *Geosci. Model Dev.*, **7**, 663–693,

783   https://doi.org/10.5194/gmd-7-663-2014.

784   Wehrli, K., B. P. Guillod, M. Hauser, M. Leclair, and S. I. Seneviratne, 2018: Assessing the

785   Dynamic Versus Thermodynamic Origin of Climate Model Biases. *Geophys. Res. Lett.*, **45**,

786   8471–8479, https://doi.org/10.1029/2018GL079220.

787   ——, ——, ——, ——, and S. I. Seneviratne, 2019: Identifying Key Driving Processes of

788   Major Recent Heat Waves. *J. Geophys. Res. Atmospheres*, **124**, 11746–11765,

789   https://doi.org/10.1029/2019JD030635.

790   ——, M. Hauser, and S. I. Seneviratne, 2020: Storylines of the 2018 Northern Hemisphere

791   heatwave at pre-industrial and higher global warming levels. *Earth Syst. Dyn.*, **11**, 855–

792   873, https://doi.org/10.5194/esd-11-855-2020.

793 Wiltshire, K. H., and Coauthors, 2010: Helgoland Roads, North Sea: 45 Years of Change.

794 *Estuaries Coasts*, **33**, 295–310, https://doi.org/10.1007/s12237-009-9228-y.

795 Woollings, T., and Coauthors, 2018: Blocking and its Response to Climate Change. *Curr. Clim.*

796 *Change Rep.*, **4**, 287–300, https://doi.org/10.1007/s40641-018-0108-z.

797 Zhang, K., and Coauthors, 2014: Technical note: On the use of nudging for aerosol-climate

798 model intercomparison studies. *Atmos. Chem. Phys.*, **14**, 8631–8645,

799 https://doi.org/10.5194/acp-14-8631-2014.

800 Zhou, C., K. Wang, D. Qi, and J. Tan, 2019: Attribution of a record-breaking heatwave event

801 in summer 2017 over the yangtze river delta. *Bull. Amer. Meteor. Soc.*, **100**, S97–S103,

802 https://doi.org/10.1175/BAMS-D-18-0134.1.

803

804

805

806

807

808

809

810

811

812

813

FIGURES

250 hPa Wind 16 June 2017
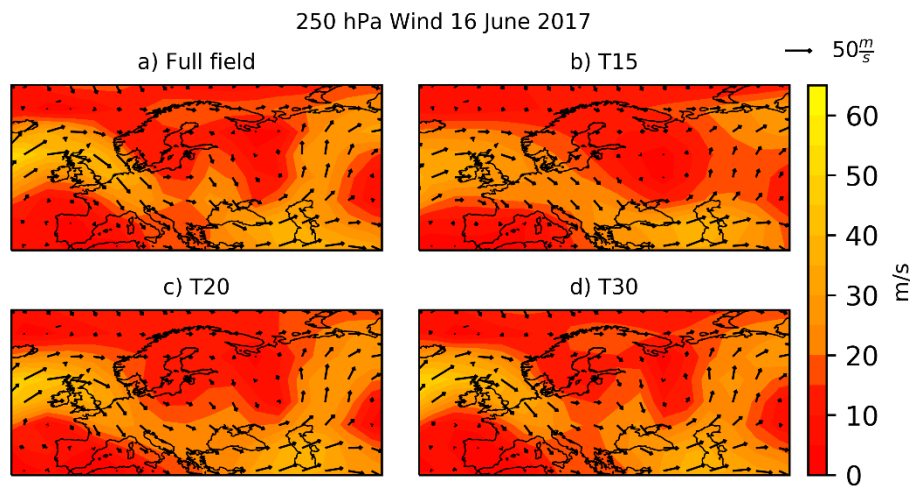
815
816
817   Figure 1. Daily mean winds at 250 hPa on 16 June 2017 from ERA5 for (a) the original field

818   and for truncated fields retaining only total wavenumbers up to (b) 15, (c) 20 and (d) 30.
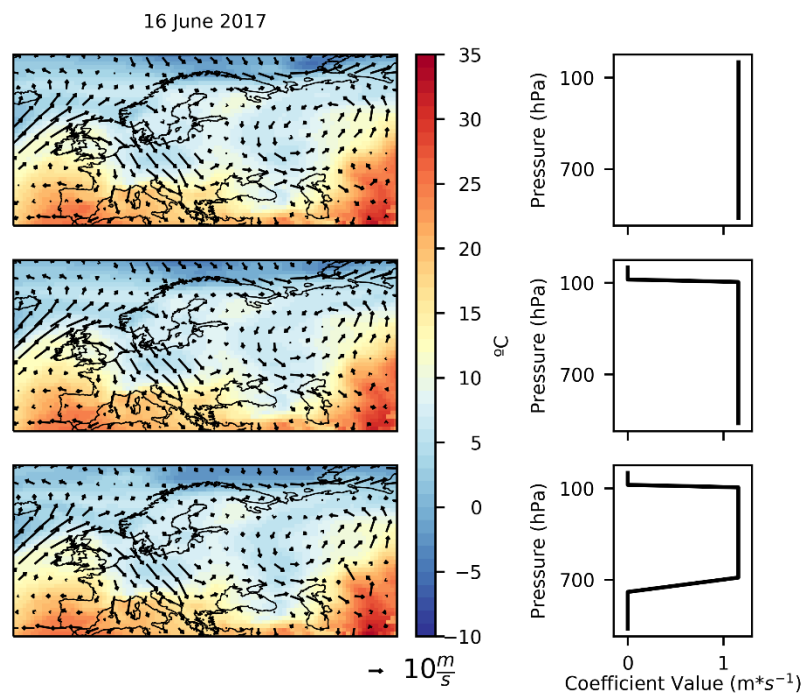
819

820   Figure 2. Daily mean temperature (shading) and winds (arrows) at 850 hPa on 16 June 2017

821   (left) for different vertical profiles indicated in the right panels. For all simulations vorticity

822   and divergence were nudged up to total wavenumber 20 with a nudging time scale of τ=24h.

37

18 July 2018

a) τ=6 hours   → $10\frac{m}{s}$

b) τ=24 hours
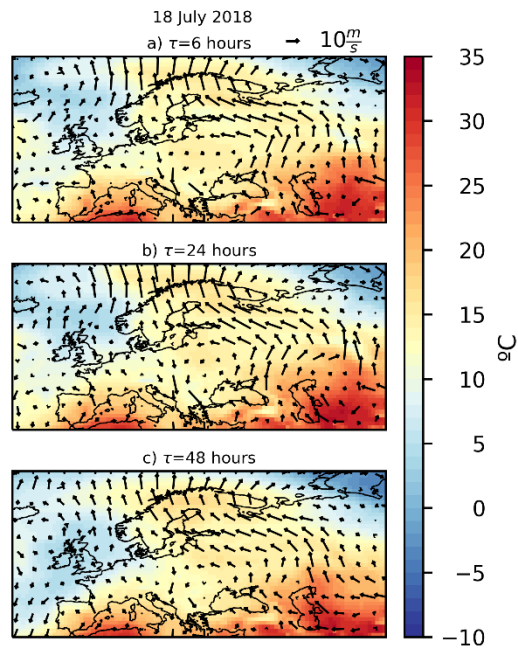
c) τ=48 hours

823

824   Figure 3. Temperature (shading) and winds (arrows) at 850 hPa on 18 July 2018 using different

825   e-folding times: (a) 6 hours, (b) 24 hours, and (c) 48 hours. For all simulations vorticity and

826   divergence were nudged up to total wavenumber 20 using the vertical profile shown in the

827   lower right panel of Fig. 2.

828

829
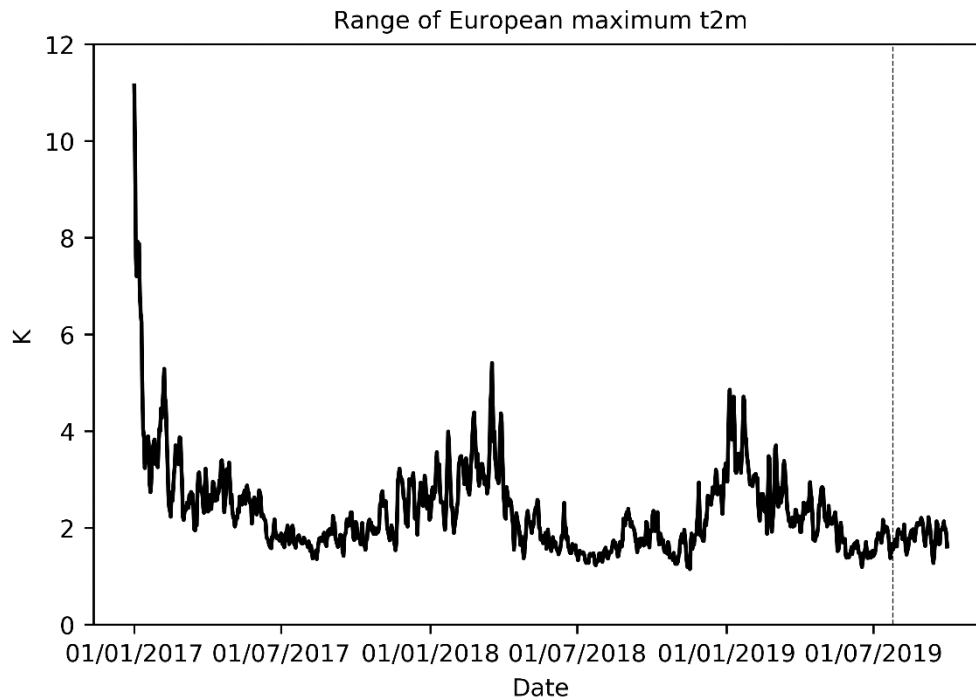
Figure 4. Temporal evolution of the range of daily maximum t2m for Europe (See Fig. A3d

for more details on the region). The range is computed as the difference between the daily

maximum and minimum values of the five ensemble members for each day. Larger values

indicate that maximum t2m is less well constrained by the nudging. The peak of the

European heatwave on 25 July 2019 is marked by the vertical dashed line.

835

25 July 2019

Nudged Simulations   ERA5

a) Z500 b)

c) T850 d)

e) max t2m f)

g) SST h)

i) Volumetric soil moisture at level 1 j)

k) Total Cloud Cover l)

836
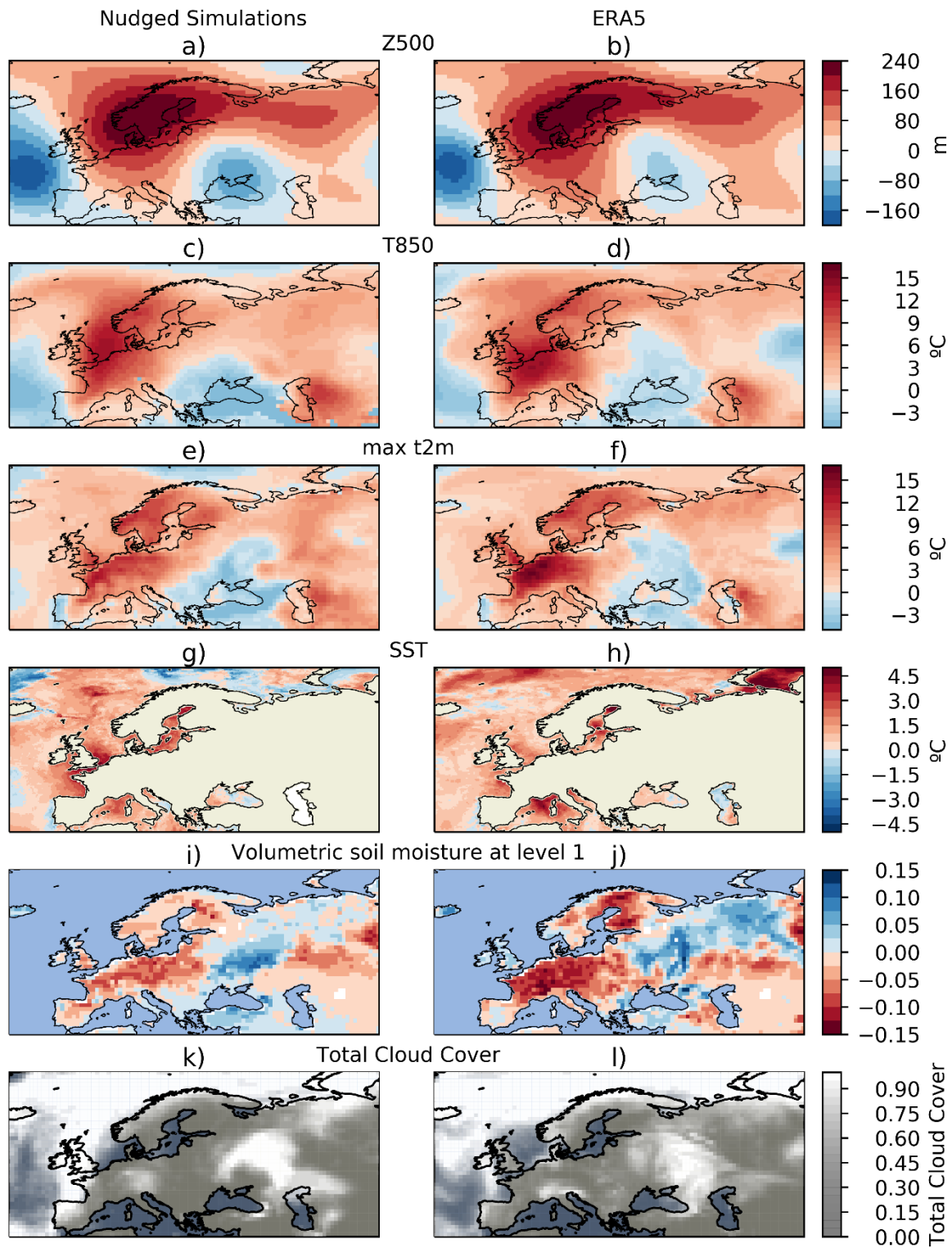
Figure 5. Anomalies from (a,c,e,g,i) the nudged present-day simulations and (b,d,f,h,j,l) ERA5

for 25 July 2019 and different variables: (a,b) 500 hPa geopotential height, (c,d) 850 hPa

40

839   temperature (e,f) maximum 2m temperature, (g,h) sea surface temperature, and (i,j) volumetric

840   soil moisture in the 1st layer. Anomalies were computed as the differences of daily value from

841   the 15-days moving average in the 1981–2010 period. Total cloud cover on 25 July 2019 for

842   (k) the nudged present-day simulations and (l) ERA5.

843

2018-2019 Summers Pearson correlation

844
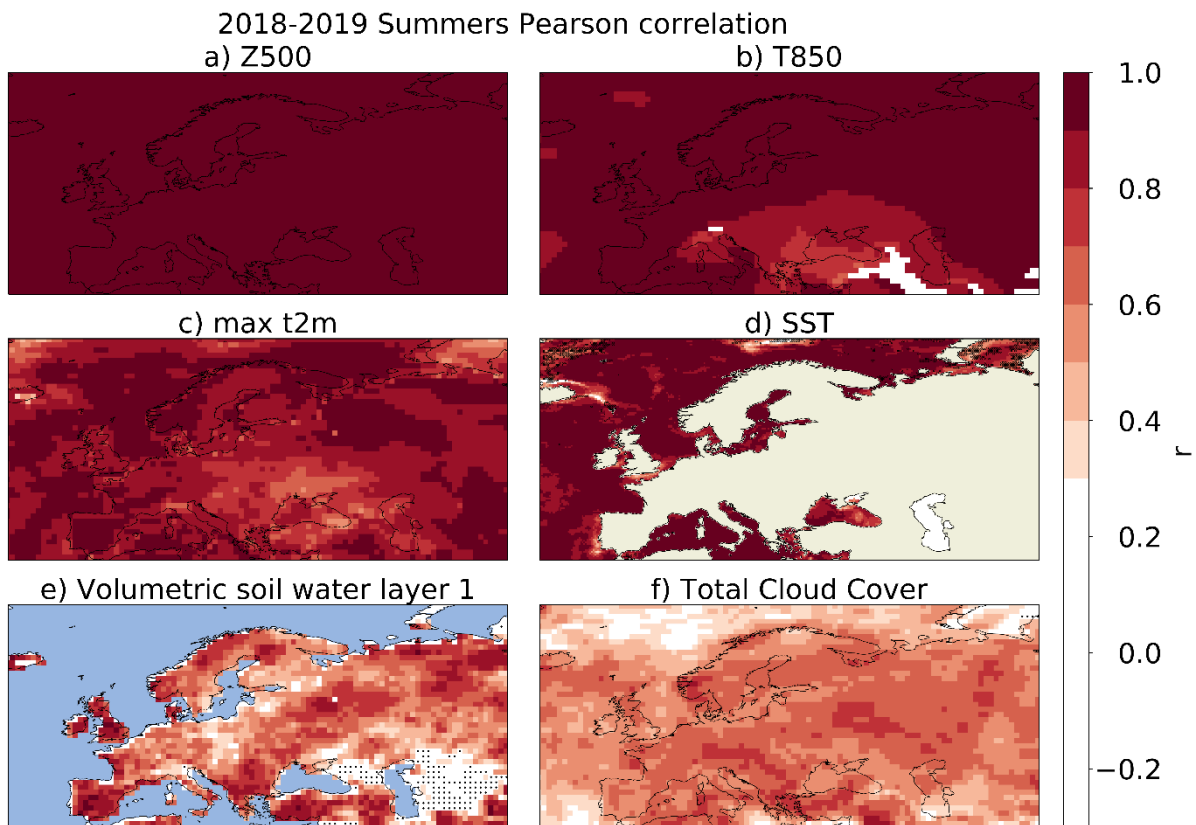
845   Figure 6. Pearson correlation between present-day simulations and ERA5 for the summers of

846   2018 and 2019 using daily fields: (a) 500 hPa geopotential height, (b) 850 hPa temperature,

847   (c) maximum 2m temperature, (d) sea surface temperature, (e) volumetric soil moisture in the

848   1st layer, (f) total cloud cover. Grid points with non-significant correlation are shown with dots.

849

850

851

File generated with AMS Word template 1.0

a) Europe   b) Germany

852
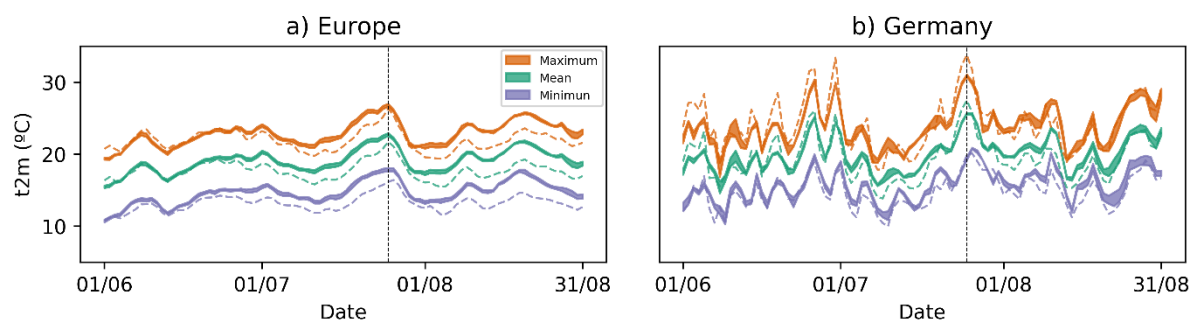
Figure 7. Seasonal evolution of daily minimum (purple), daily mean (green) and daily maximum (orange) 2m temperature for (a) Europe and (b) Germany and the period 1 June to 31 August 2019. Results are shown for the nudged simulations under present-day conditions (shading) as well as for ERA5 reanalysis data (dashed lines). Shading denotes the min/max range of values obtained from the respective 5-member ensembles. The peak of the European heatwave on 25 July 2019 is marked by the vertical dashed line.

859

860
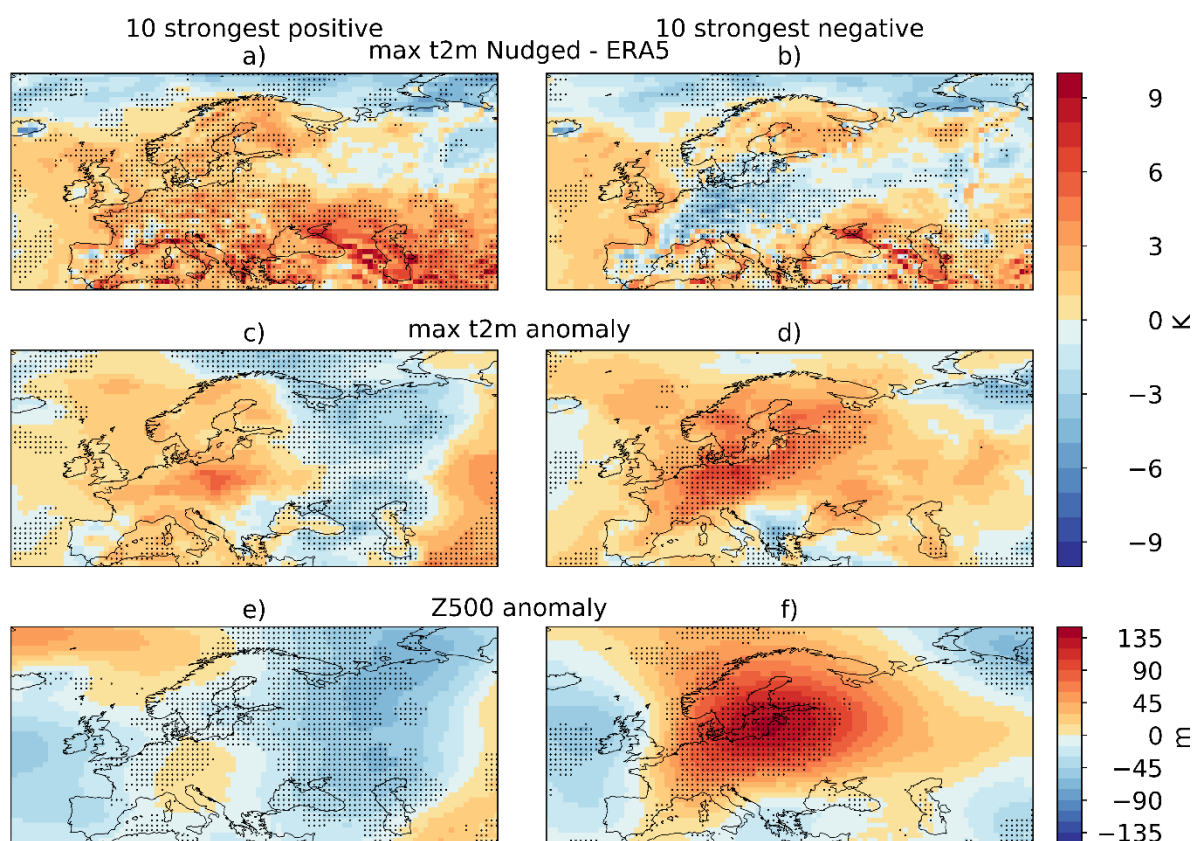
Figure 8. (a,b) max t2m differences between the nudged present-day simulations and ERA5, (c,d) max t2m anomaly and (e,f) Z500 anomaly for the ten days with (a,c,e) strongest positive and (b,d,f) negative Germany maximum t2m differences between the simulations and ERA5. The summers of 2018 and 2019 were included. Grid points where the differences are significant are shown with points.
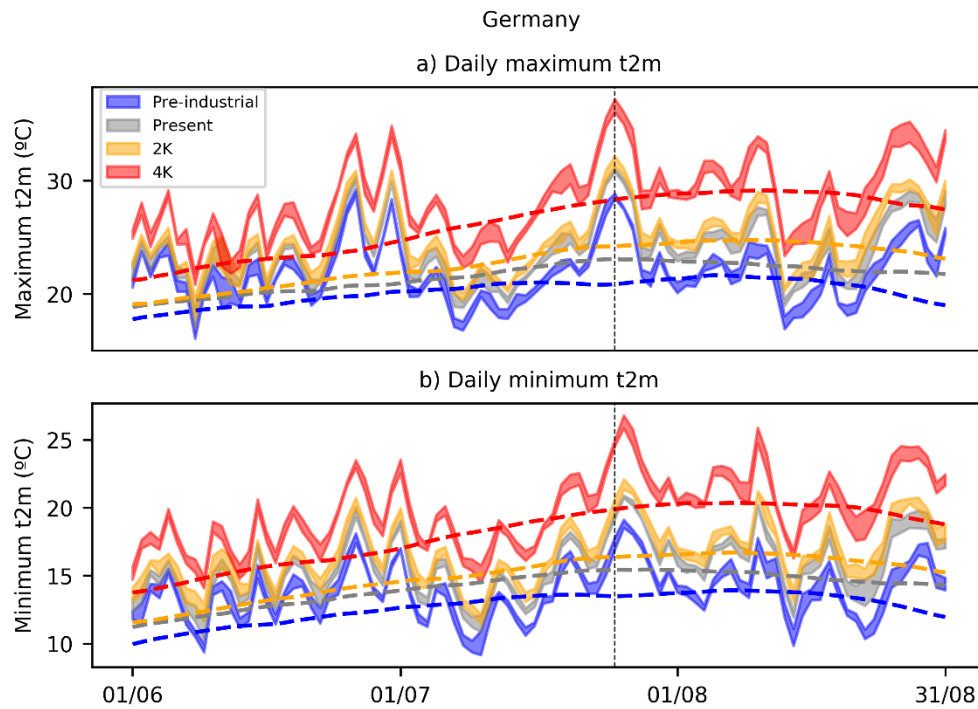
Figure 9. Seasonal evolution of (a) daily maximum and (b) minimum t2m averaged for Germany and different climates (pre-industrial in blue, present-day in grey, +2K in orange and +4K in red). Shading spans the min/max range of values obtained from the 5-member ensembles and dashed lines show the mean from the free-run. Differences are shown in Fig. A5. The peak of the European heatwave on 25 July 2019 is marked by the vertical dashed line.

885

a) North Sea

Pre-industrial
Present
2K
4K

SST (ºC)

b) German Bight

SST (ºC)

01/06   01/07   01/08   31/08
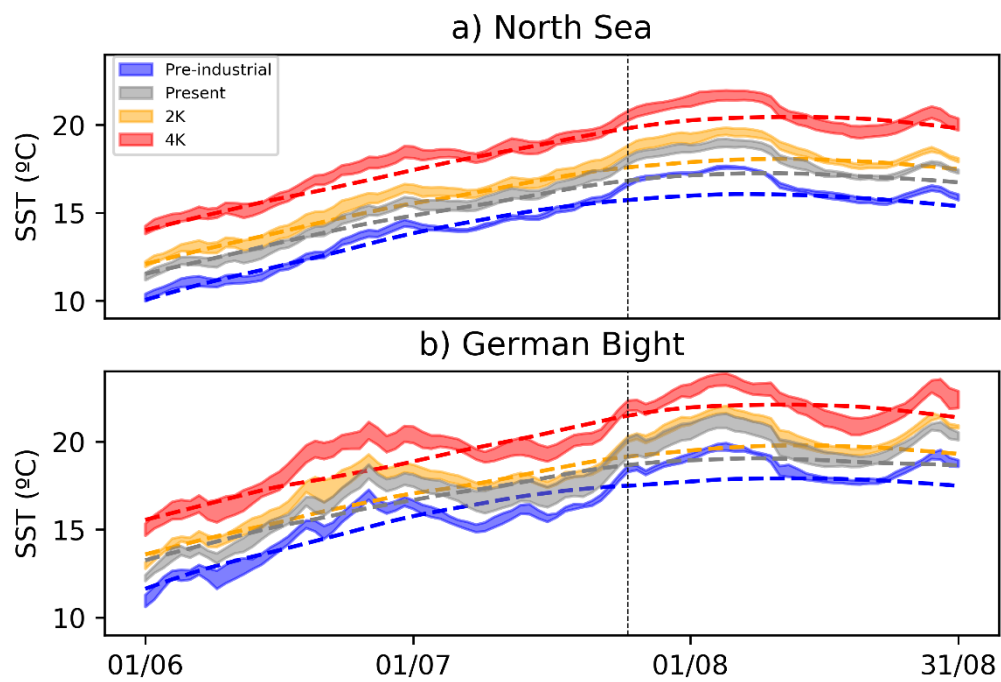
894   Figure 10. Same as Fig. 9, except for sea surface temperature in (a) the North Sea and (b) the

895   German Bight. The peak of the European heatwave on 25 July 2019 is marked by the vertical

896   dashed line.

897

25 July 2019
a) 4K-Present
b) 2K-Present
c) Present-Preindustrial
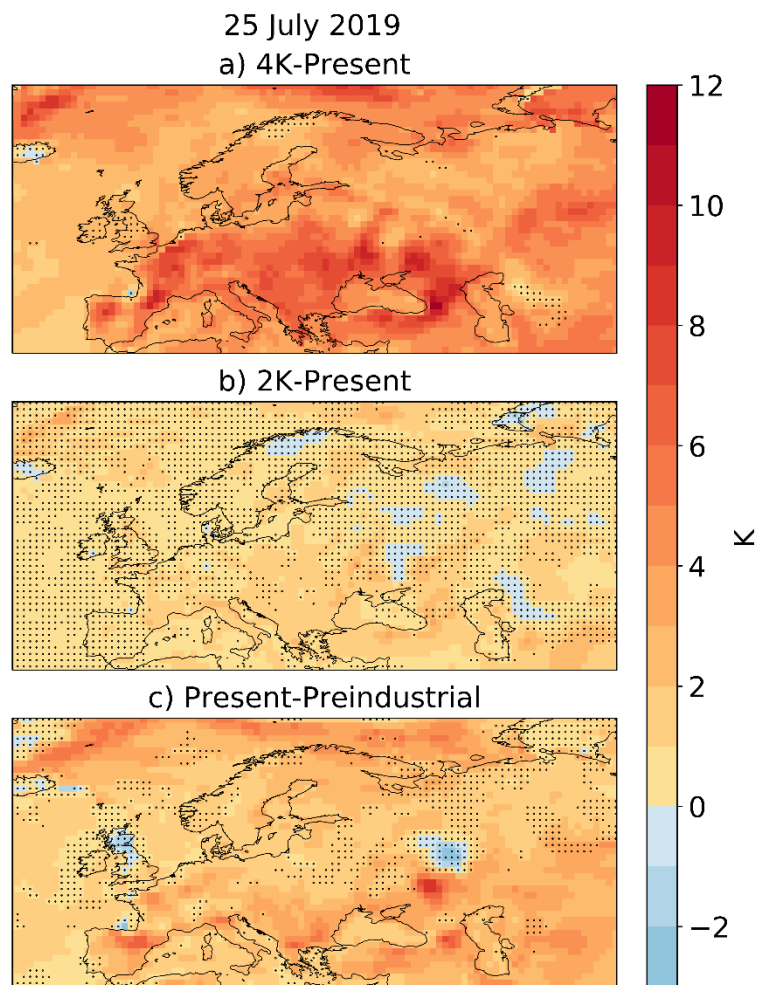
899   Figure 11. Daily maximum t2m differences on 25 July 2019: (a) +4K minus present-day, (b)

900   +2K minus present-day, and (c) present-day minus pre-industrial. Locations where the

901   ensembles   overlap   between   different   climates   are   indicated   with   points.

902

903

904

905

Germany
a) Soil Wetness
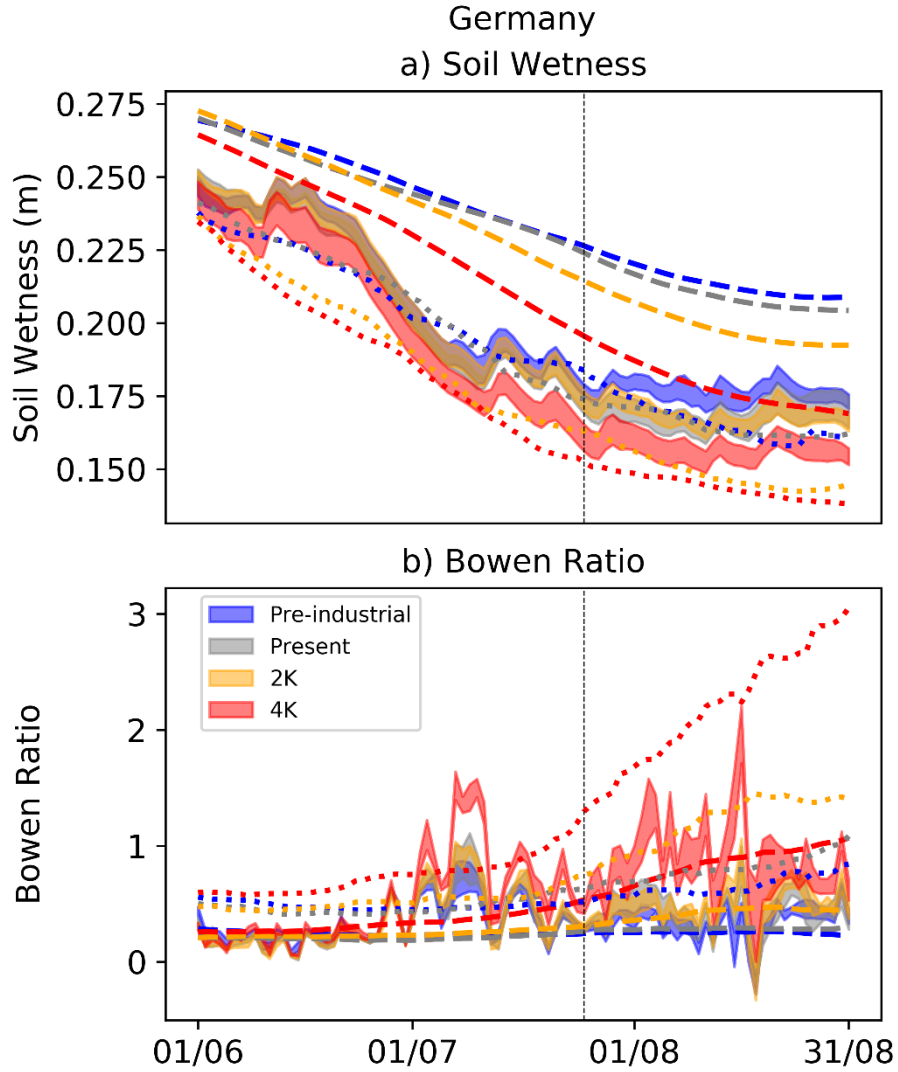
b) Bowen Ratio

Figure 12. Seasonal evolution of (a) soil wetness and (b) Bowen ratio in Germany between 1 June to 31 August 2019 in different climates (pre-industrial in blue, present-day in yellow and 2K and 4K warmer worlds in orange and red, respectively). Shading spans the min/max range of values obtained by the respective 5-member ensembles. Dashed lines show the mean and dotted lines the 5th and 95th quantile for Soil Wetness and Bowen Ratio respectively. The peak of the European heatwave on 25 July 2019 is marked by the vertical dashed line.

915
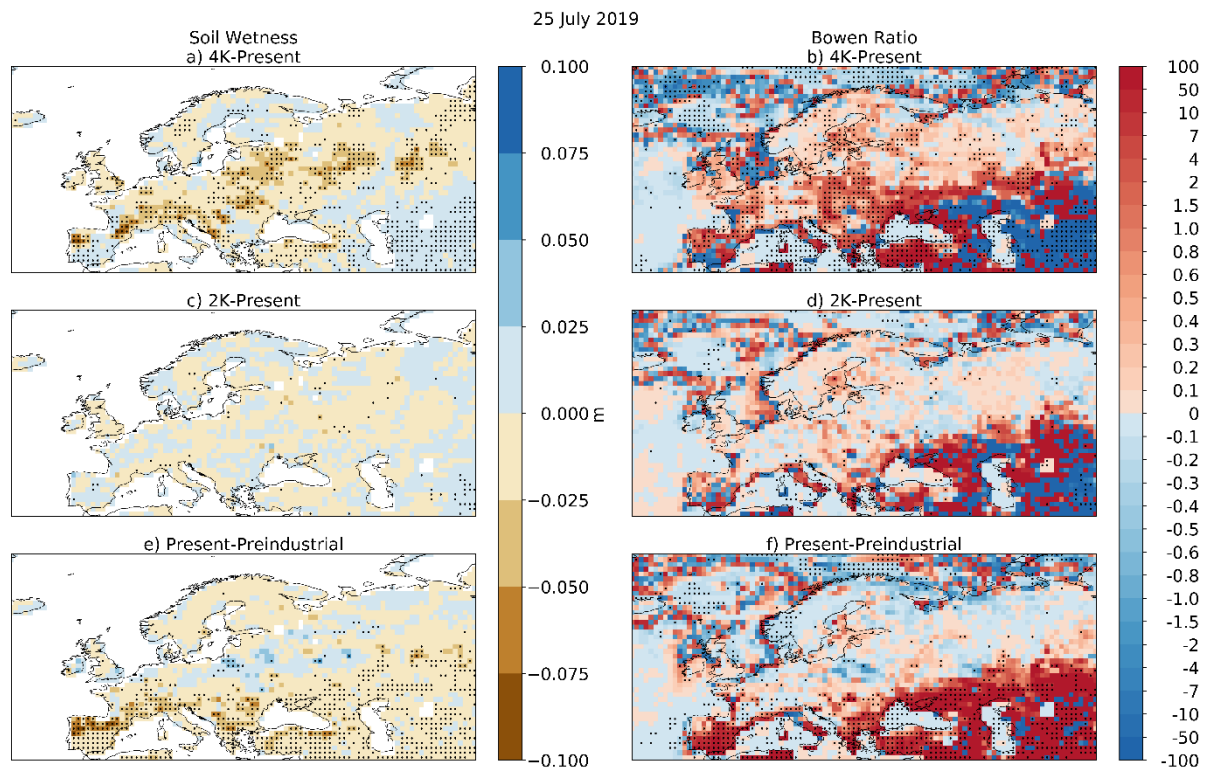
917 Figure 13. (a,c,e) Soil wetness and (b,d,f) Bowen ratio differences between (a,b) 4K warmer

918 and present, (c,d) 2K warmer and present and (e,f) present and preindustrial climates on 25

919 July 2019. Locations where the two ensembles do not overlap are indicated by dots.

920
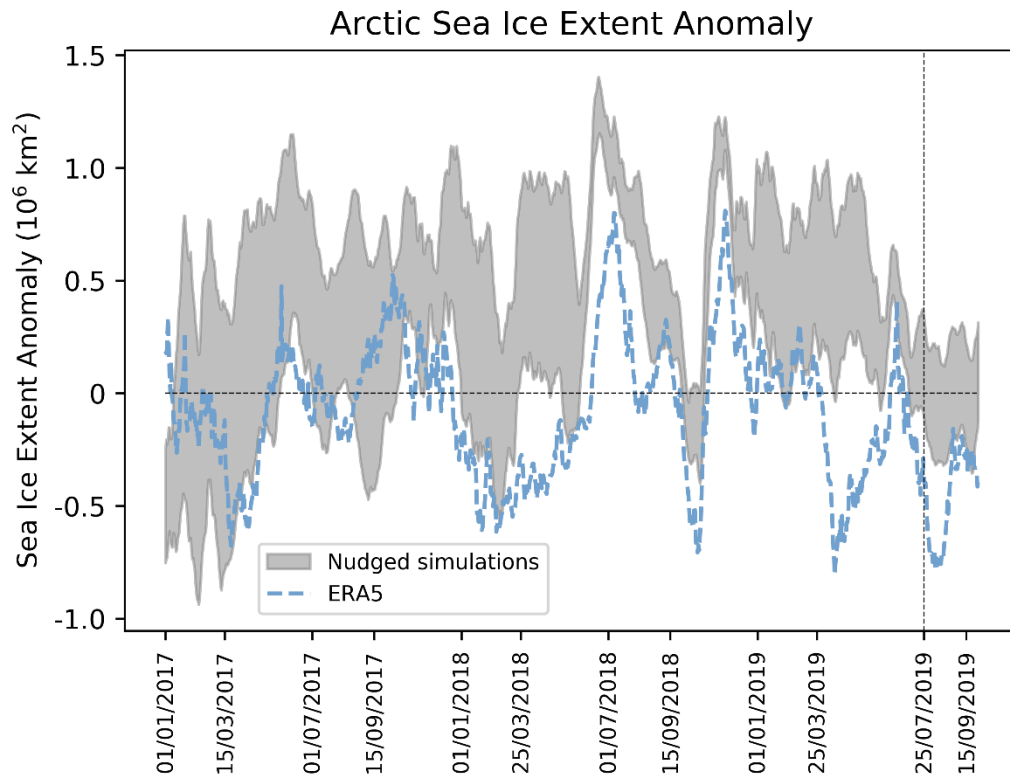
Figure 14. Arctic sea ice extent anomalies (climatology computed using the 2007–2016 period) from ERA5 (blue solid line) and the present-day nudged simulation. The peak of the European heatwave on 25 July 2019 is marked by the vertical dashed line.

921

922

923

924

925

926

927

928

25 July 2019
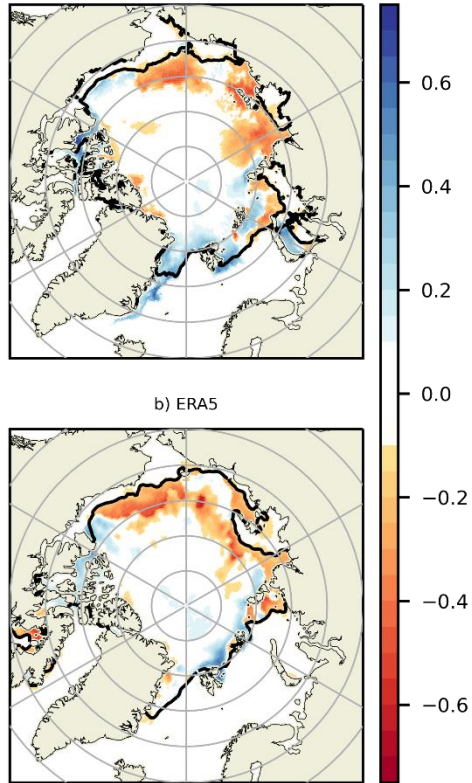
a) AWI-CM

b) ERA5

929

930   Figure 15. SIC anomalies (climatology computed using the 2007-2016 period) on 25th July

931   2019 from (a) AWI-CM nudged simulations and (b) ERA5. Black contours show the

932   respective climatological 15% sea-ice concentration.

933
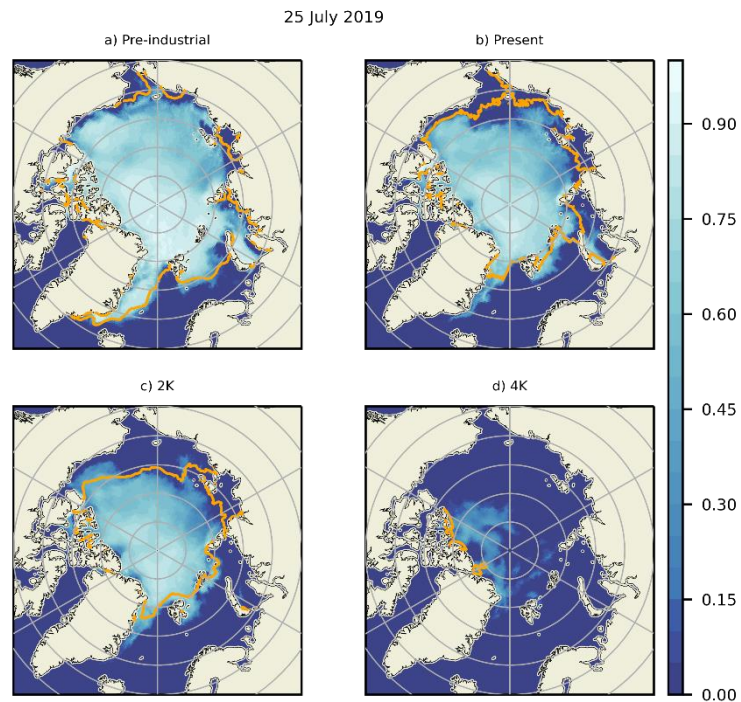
25 July 2019

Figure 16. Sea ice concentration on 25th July 2019 from AWI-CM nudging experiments for different climates: (a) pre-industrial, (b) present-day, (c) 2K warmer world and (d) 4K warmer world. Orange contours show the respective climatological 15% sea-ice concentration contour.
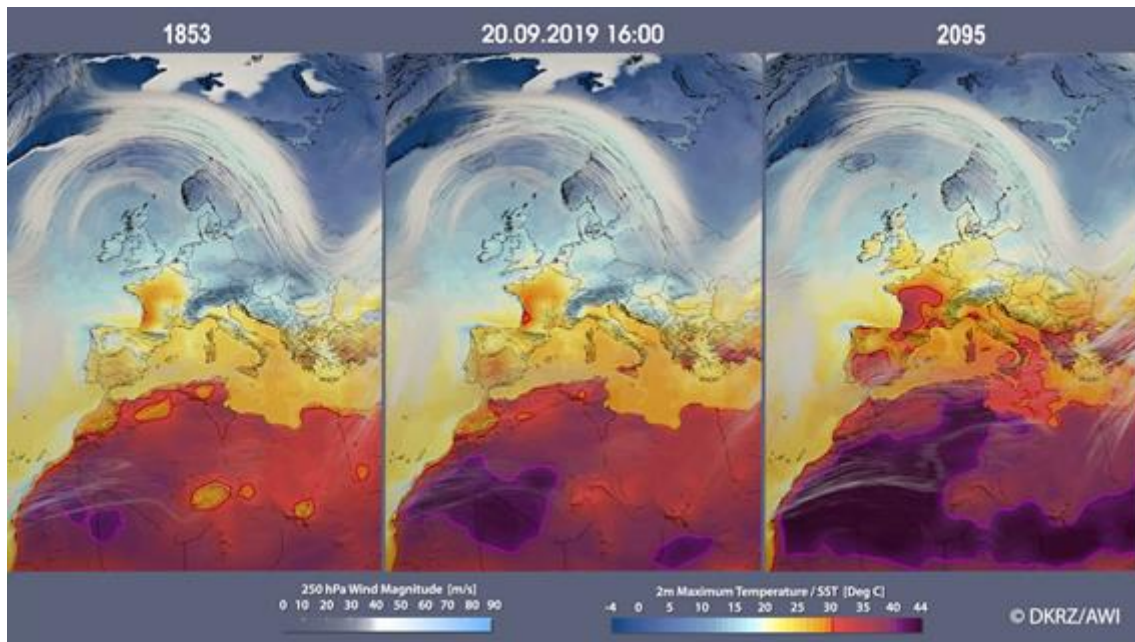
Figure 17. Storyline simulations of maximum 2m temperature, sea-surface temperature, sea ice and 250 hPa winds at 1600 UTC on 20 September 2019: (left) for a pre-industrial climate, (middle) present-day conditions, and (right) a 4K warmer world. 30C and 40C isotherms are indicated by red and purple bold contours, respectively.
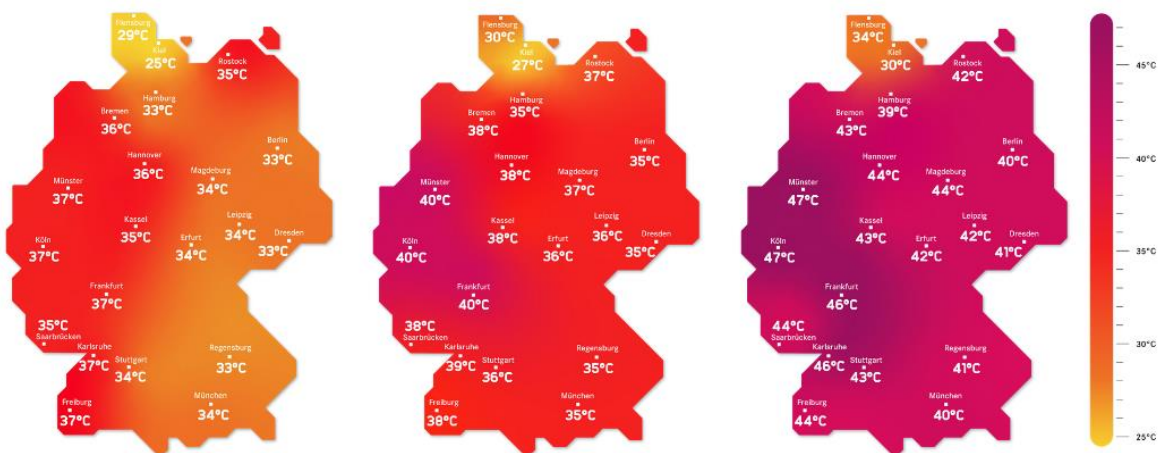
Figure 18. Schematic maps of 2m temperature for weather conditions in Germany at 1500 UTC on 25 July 2019: (left) for a pre-industrial climate, (middle) present-day conditions, and (right) a 4K warmer world. The maps have been produced by graphic designers of the communication

52

950   team of the Helmholtz Climate Initiative using observed values for the locations shown on the

951   map and by adding temperature increments from the storyline scenarios for pre-industrial and

952   4K warmer conditions.

Supplemental Material.
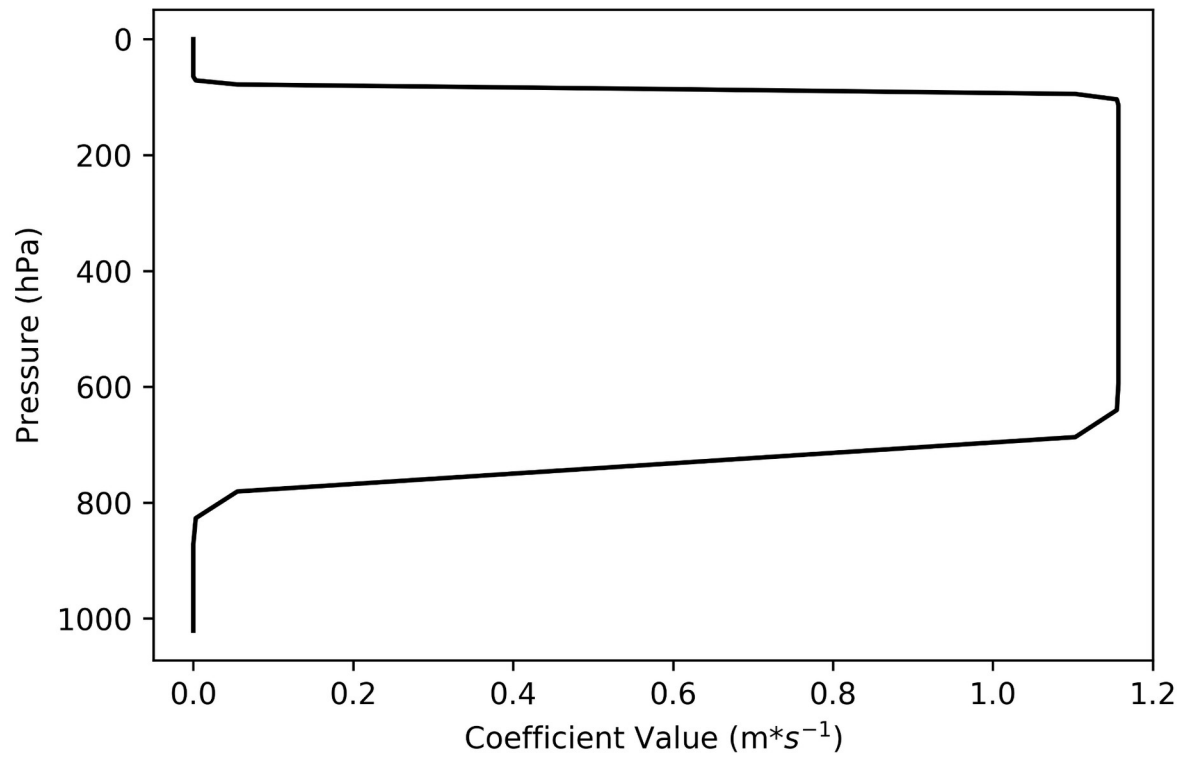
Figure S1. Vertical profile of the nudging coefficient used in our simulations.
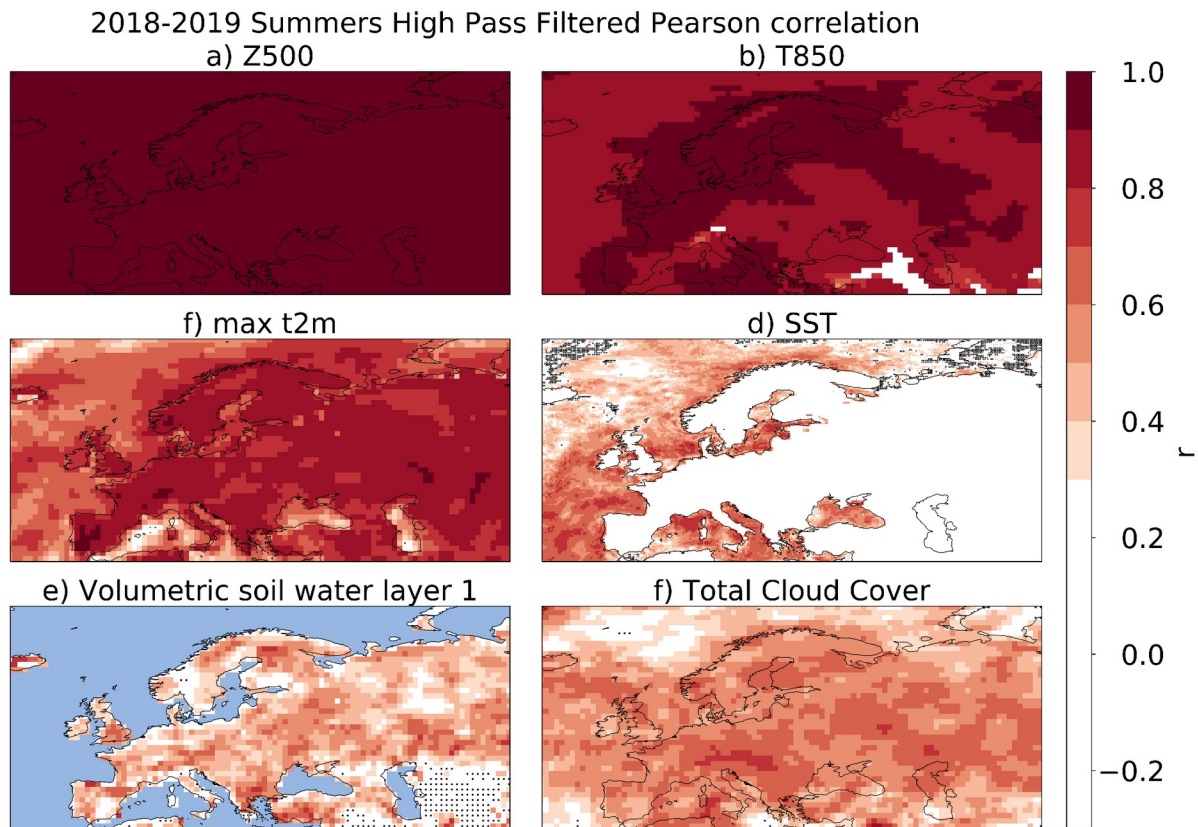
2018-2019 Summers High Pass Filtered Pearson correlation
a) Z500
b) T850
f) max t2m
d) SST
e) Volumetric soil water layer 1
f) Total Cloud Cover

Figure S2. As Fig.6 but computed after having removed low-frequency variability (15-days running mean).
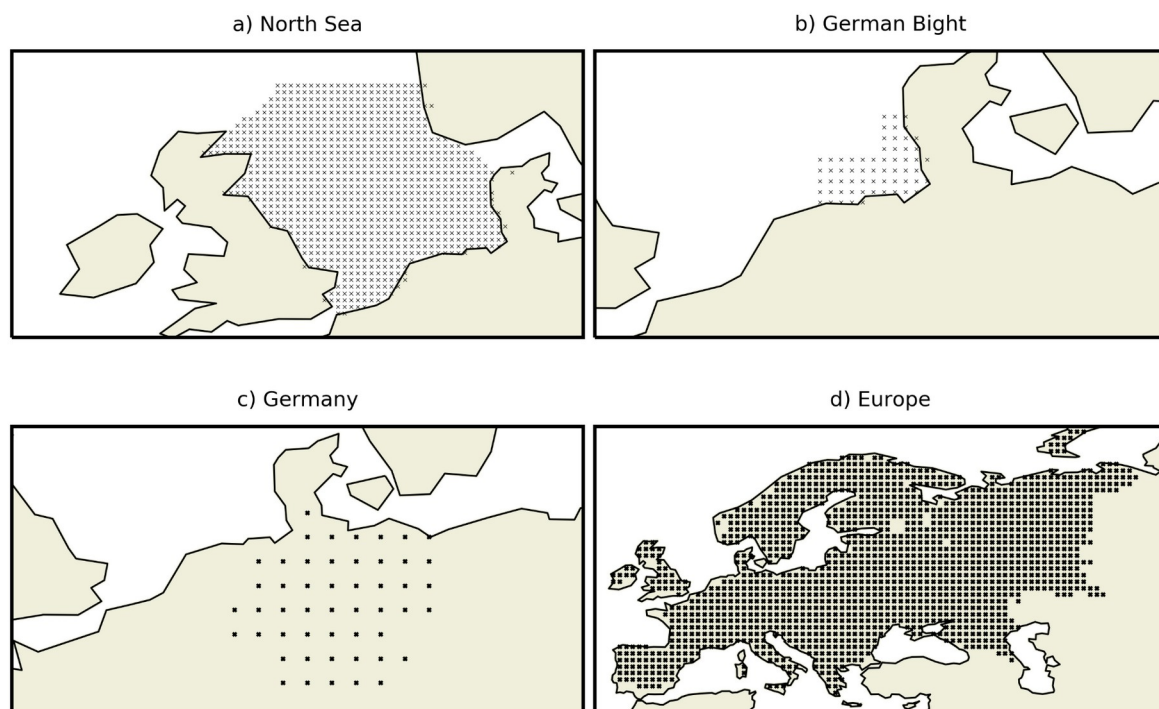
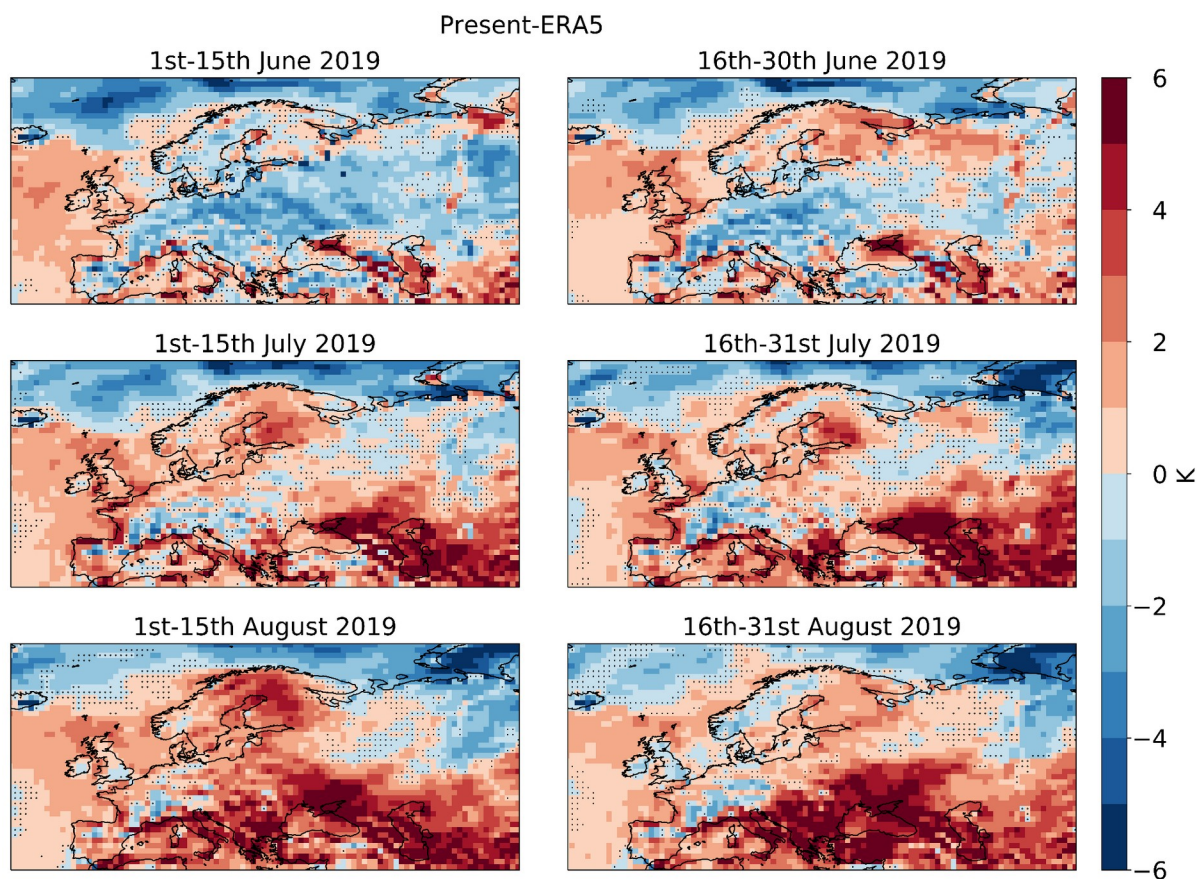Figure S3. Illustration of the different areas used in this study.

Figure S4. Evolution of the mean maximum t2m differences (in ºC) between the present-day nudging simulations and ERA5 in summer 2019. Locations where the ensemble overlaps with ERA5 are indicated by dots.
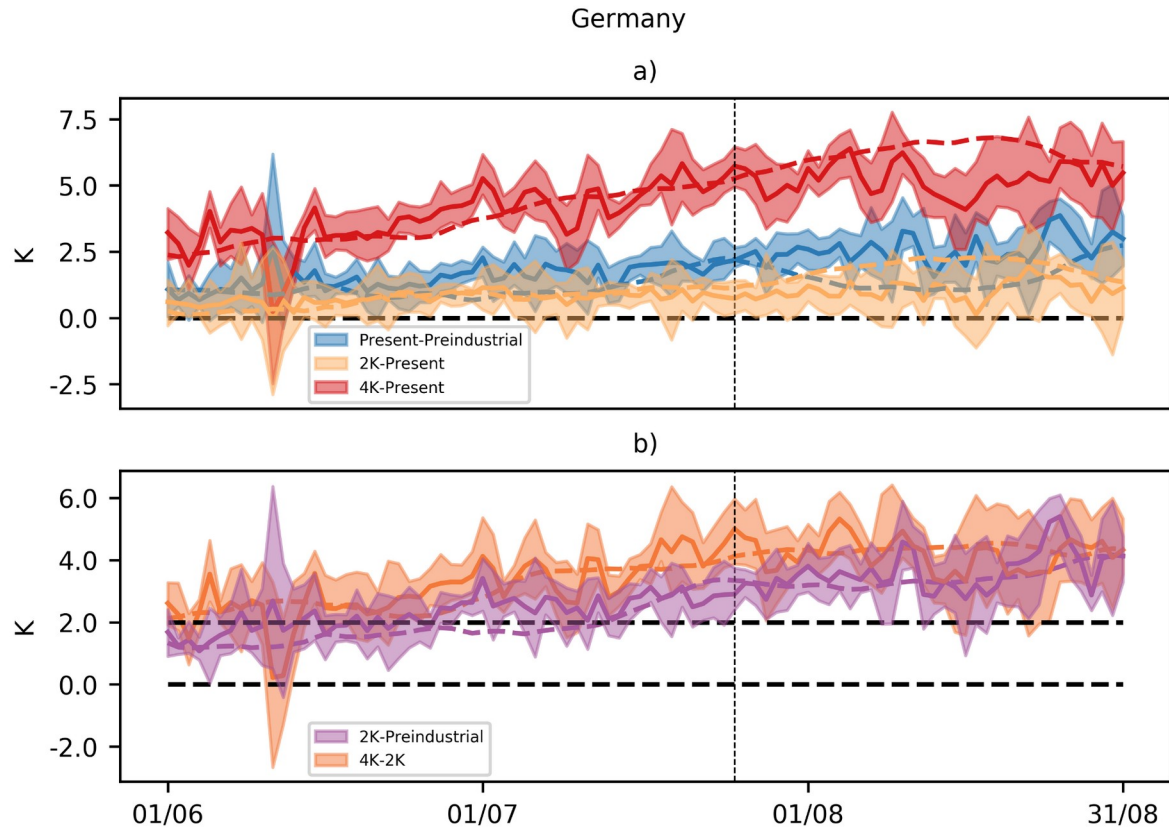
Figure S5. Seasonal evolution of daily maximum t2m differences averaged for Germany heatwave different climates. (a) Present-day minus pre-industrial (blue), +2K minus present-day (yellow), and +4K minus present-day (red). (b) +2K minus pre-industrial (purple) and +4K minus +2K (orange). Shading spans the min/max range of values obtained by the respective 5-member ensembles. Solid and dashed lines show differences for the ensemble mean and the climatology (from the free-run), respectively. The peak of the European heatwave on *25 July 2019 is marked by the vertical dashed line.*
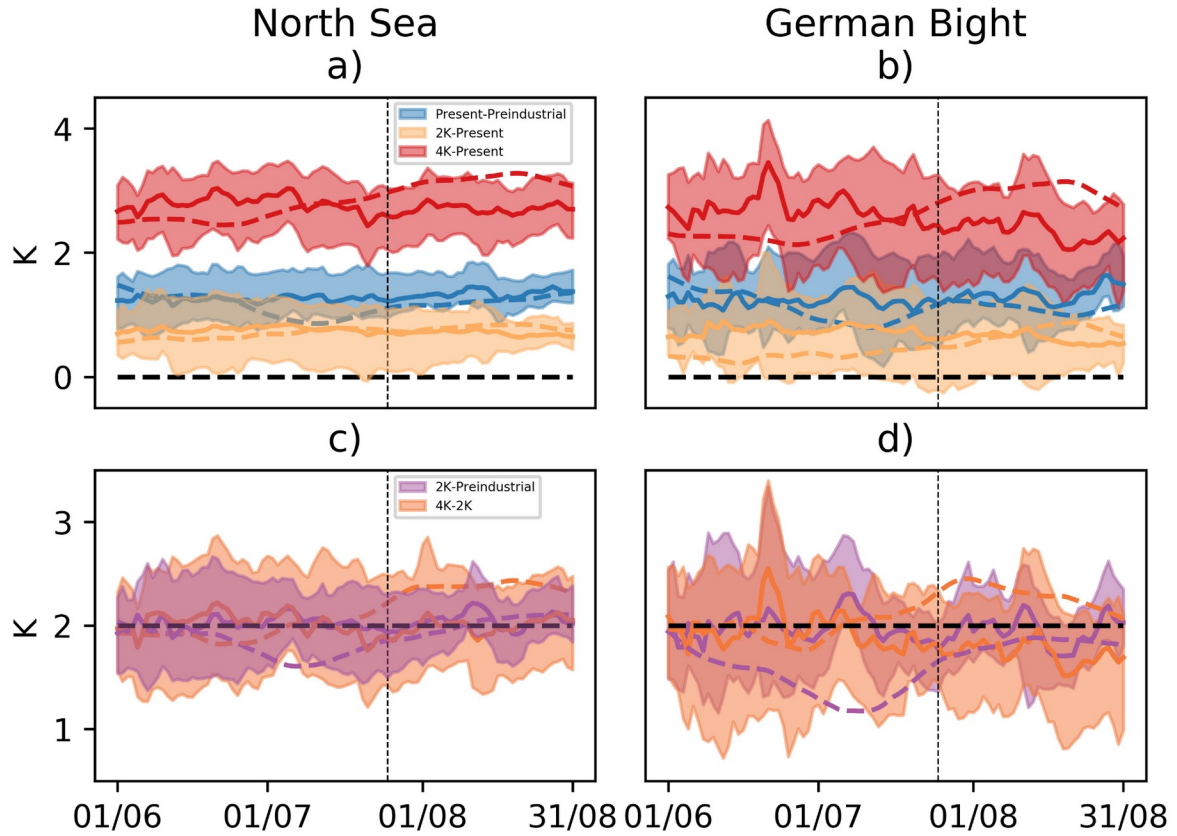
Figure S6. Seasonal evolution of SST differences averaged for (a,c) the North Sea and (b,d) German Bight between different climates. (a,b) Present-day minus pre-industrial (blue), +2K minus present-day (yellow), and +4K minus present-day (red). (c,d) +2K minus pre-industrial (purple) and +4K minus +2K (orange). Shading spans the min/max range of values obtained by the respective 5-member ensembles. Solid and dashed lines show the ensemble mean and the climatology (from the free-run), respectively. The peak of the European heat wave on *25 July 2019 is marked by the vertical dashed line.*